Article

Neuron

Neuronal Activity and CaMKII Regulate Kinesin-Mediated Transport of Synaptic AMPARs

Highlights

- AMPAR transport is regulated by synaptic transmission, VGCCs and CaMKII
- A critical target of CaMKII is kinesin light chain 2 (vKLC1)
- Glutamate-gated currents are disrupted in CaMKII mutants
- Optegenetic experiments reveal a critical role for CaMKII in synaptic plasticity

Authors

Frédéric J. Hoerndli, Rui Wang, ..., David M. Madsen, Andres V. Maricq

Correspondence

maricq@biology.utah.edu

In Brief

Using real-time in vivo imaging and electrophysiology, Hoerndli et al. demonstrate that UNC-43/CaMKII regulates the delivery and removal of synaptic AMPA receptors, and is required for the homeostatic control of synaptic strength and activity dependent synaptic plasticity.

Hoerndli et al., 2015, Neuron *86*, 457–474
April 22, 2015
http://dx.doi.org/10.1016/j.neuron.2015.03.011

CellPress

Neuron
Article

Neuronal Activity and CaMKII Regulate Kinesin-Mediated Transport of Synaptic AMPARs

Frédéric J. Hoerndli,[1] Rui Wang,[1] Jerry E. Mellem,[1] Angy Kallarackal,[1] Penelope J. Brockie,[1] Colin Thacker,[1] David M. Madsen,[1] and Andres V. Maricq[1,*]
[1]Department of Biology and Center for Cell and Genome Science, University of Utah, Salt Lake City, UT 84112-0840, USA
*Correspondence: maricq@biology.utah.edu
http://dx.doi.org/10.1016/j.neuron.2015.03.011

SUMMARY

Excitatory glutamatergic synaptic transmission is critically dependent on maintaining an optimal number of postsynaptic AMPA receptors (AMPARs) at each synapse of a given neuron. Here, we show that presynaptic activity, postsynaptic potential, voltage-gated calcium channels (VGCCs) and UNC-43, the *C. elegans* homolog of CaMKII, control synaptic strength by regulating motor-driven AMPAR transport. Genetic mutations in *unc-43*, or spatially and temporally restricted inactivation of UNC-43/CaMKII, revealed its essential roles in the transport of AMPARs from the cell body and in the insertion and removal of synaptic AMPARs. We found that an essential target of UNC-43/CaMKII is kinesin light chain and that mouse CaMKII rescued *unc-43* mutants, suggesting conservation of function. Transient expression of UNC-43/CaMKII in adults rescued the transport defects, while optogenetic stimulation of select synapses revealed CaMKII's role in activity-dependent plasticity. Our results demonstrate unanticipated, fundamentally important roles for UNC-43/CaMKII in the regulation of synaptic strength.

INTRODUCTION

Glutamate mediates the majority of excitatory neurotransmission in the brain by activating the AMPA-subtype of ionotropic glutamate receptors (iGluRs). Consequently, many studies of synaptic plasticity have focused on the mechanism of local changes in the composition and number of postsynaptic AMPA receptors (AMPARs), with particular focus on changes that underlie the phenomena of long-term potentiation (LTP) and long-term depression (LTD) (Anggono and Huganir, 2012; Kerchner and Nicoll, 2008; Kessels and Malinow, 2009; Malenka and Bear, 2004). These potentiation protocols cause local, synapse-specific changes in postsynaptic receptors and thus modify the strength of neurotransmission. Additionally, information processing by neural circuits is dependent on maintaining an optimal strength of synaptic inputs in the face of constant perturbations. Thus, postsynaptic receptor numbers are tightly constrained by homeostatic mechanisms (Davis, 2013; Turrigiano, 2008). However, the molecular mechanisms that maintain the optimal number of AMPARs at a given synapse are still not well understood. Even less understood is the logistical problem of maintaining AMPAR numbers at the hundreds to thousands of independently functioning synapses that are distributed along dendritic branches that can extend hundreds of microns from the neuronal cell body.

We approached the question of how AMPARs are maintained at synapses using an experimental design that allowed us to integrate in vivo cell biological and electrophysiological studies in *C. elegans*. A subset of the 302 neurons in the *C. elegans* nervous system communicate by the synaptic release of glutamate and these neurons contribute to specific behaviors (de Bono and Maricq, 2005). In particular, interneurons that participate in the control of worm movement and avoidance responses express the GLR-1 AMPAR signaling complex, which is composed of multiple receptor and auxiliary subunits, and is responsible for fast postsynaptic glutamate-gated current. In mutants where a component of the complex has been disrupted, such as the GLR-1 subunit, the ratio of forward to backward movement is altered, thus disrupting foraging behavior (de Bono and Maricq, 2005; Zheng et al., 1999) as well as the avoidance response to tactile and osmotic stimuli (Hart et al., 1995; Maricq et al., 1995). We identified many of the molecular components of the GLR-1 signaling complex, including the GLR-2 AMPAR subunit, and the auxiliary proteins SOL-1, SOL-2, and STG-2, and determined how they contribute to postsynaptic function and the control of behavior (Brockie et al., 2001, 2013; Mellem et al., 2002; Walker et al., 2006b; Wang et al., 2008, 2012; Zheng et al., 2004, 2006).

Recently, we demonstrated that evolutionarily conserved kinesin-1 microtubule-dependent motors mediate the delivery and removal of postsynaptic AMPARs. In *unc-116* (KIF5) mutants, the active transport of GLR-1 is abolished, and the peak amplitude of glutamate-gated current greatly reduced (Hoerndli et al., 2013). These findings have important implications for synaptic function and plasticity because kinesin motors, and their GLR-1 cargo, are distributed along the length of a neuronal process and can rapidly repopulate synapses with AMPARs (Hoerndli et al., 2013). Indeed, each synapse is at most only a few seconds removed from motors transporting AMPAR cargo, raising the question of how neurons regulate the motor-driven delivery and removal of synaptic receptors.

A candidate protein for the regulation of AMPAR transport is CaMKII, a Ca^{2+}-dependent kinase with diverse cellular

functions. With respect to synaptic transmission, CaMKII is recognized as a key synaptic protein that is required to modify the number of synaptic AMPARs in response to LTP and LTD stimulation protocols (Hell, 2014; Nicoll and Roche, 2013; Shonesy et al., 2014). In *C. elegans*, the *unc-43* gene encodes the sole CaMKII homolog (Reiner et al., 1999; Rongo and Kaplan, 1999). In *unc-43* loss-of-function (*lf*) mutants, GLR-1 accumulates in neuronal cell bodies suggesting that UNC-43/CaMKII might have a role in GLR-1 transport (Rongo and Kaplan, 1999). We now demonstrate that voltage-gated Ca^{2+} channels (VGCCs) and CaMKII regulate activity-dependent transport of synaptic AMPARs. Additionally, using an optogenetics strategy, we demonstrate the dependence of synapse-specific plasticity on CaMKII. Remarkably, we find that AMPAR transport, AMPAR-mediated currents, and the regulation of synaptic strength are all disrupted in *unc-43/CaMKII* mutants. Our findings indicate that the number of functional postsynaptic AMPARs is tightly regulated by CaMKII and suggest that synaptic plasticity is controlled in part by regulated motor-driven transport.

RESULTS

Neuronal Silencing Dramatically Reduces AMPAR Transport

To determine the role of neuronal activity in the transport of AMPARs, we used a histamine-gated chloride channel (HisCl1) and cell-specific promoters to selectively silence (hyperpolarize) neurons (Pokala et al., 2014). Using either the *eat-4* or *flp-18* promoter to drive HisCl1 expression, we silenced presynaptic glutamatergic neurons or postsynaptic AVA neurons (Feinberg et al., 2008; Hoerndli et al., 2013) while simultaneously measuring AMPAR transport (see Experimental Procedures for details). We recorded the transport of a functional GLR-1::GFP fusion protein in the proximal processes of the AVA neurons (Figure S1A) using in vivo streaming confocal microscopy as previously described (Hoerndli et al., 2013). From these movies, we generated kymographs that revealed that AMPAR transport was markedly diminished when transgenic worms that expressed HisCl1 in presynaptic neurons (*eat-4* promoter) were treated with 10 mM $HisCl_2$ (Figure 1A). We found similar defects in mutants with a loss-of-function mutation in the EAT-4 vesicular glutamate transporter (VGlut) (Figure 1A; Figures S1B and S1D) and in transgenic worms treated with $HisCl_2$ that expressed HisCl1 in postsynaptic AVA neurons (*flp-18* promoter) (Figure 1B). Histamine treatment alone did not affect transport (Control, Figures 1A and 1B), and expression of the HisCl1 channel in neurons had no effect on AMPAR transport in the absence of $HisCl_2$ (data not shown).

Together, these results indicate that AMPAR transport is modified by changes in postsynaptic potential dependent on presynaptic glutamate release. This raised the question of how changes in postsynaptic potential regulate AMPAR transport. One possibility is that glutamatergic transmission leads to changes in the activity of VGCCs and thus the concentration of intracellular Ca^{2+}. The $\alpha 2\delta$ subunit contributes to the function of all members of the VGCC family (Dolphin, 2013). Therefore, we examined AMPAR transport in *unc-36/*$\alpha 2\delta$ mutants and found that transport was severely disrupted (Figures 1C and 1D). This result is consistent with an earlier report of altered GLR-1::GFP distribution in *unc-36* mutants (Rongo and Kaplan, 1999). We observed similar transport defects with cell-specific RNAi knockdown of *unc-36* in AVA (Figures S1C and S1D). The defects were partially rescued in transgenic *unc-36* mutants that specifically expressed a wild-type *unc-36* transgene in AVA (*unc-36(lf)* AVA rescue; Figures 1C and 1D). The partial rescue was expected given the known dependence of presynaptic release on VGCCs (Südhof, 2013). Together, these data suggest that VGCCs function in AVA to regulate AMPAR transport.

Similar to vertebrates, *C. elegans* has three classes of VGCC $\alpha 1$ subunits, but each class contains only a single homolog, e.g., L-type (EGL-19), non-L-type (UNC-2), and T-type (CCA-1) (Jeziorski et al., 2000). We also found that flux was significantly reduced in *unc-2* and *egl-19* mutants (Figures 1C and 1D). In summary, our results suggest a model where glutamatergic signaling activates postsynaptic VGCCs, thus modifying intracellular Ca^{2+} and consequently AMPAR transport. To learn more about this Ca^{2+}-signaling pathway, we turned to a candidate gene approach.

AMPAR Transport Is Dramatically Reduced in *unc-43(lf)* Mutants

Because of the known dependence of UNC-43/CaMKII on Ca^{2+}, we examined AMPAR transport in *unc-43* mutants. We found a significant decrease in GLR-1 flux in *unc-43* loss-of-function (*lf*) mutants when compared to wild-type worms (Figures 2A and 2B), with approximately 20% of flux remaining in *unc-43(lf)* mutants. We did not find that the speed of transport was dramatically altered in *unc-43* mutants (anterograde: WT, 1.67 ± 0.04 μm/s; *unc-43(lf)*, 1.35 ± 0.05 μm/s; retrograde: WT, 1.76 ± 0.07 μm/s; *unc-43(lf)*, 1.66 ± 0.17 μm/s).

We could rescue the defective transport in *unc-43(lf)* transgenic mutants by selectively expressing a wild-type *unc-43* transgene in AVA (*unc-43(lf)* rescue; Figures 2A and 2B), indicating that UNC-43/CaMKII has a cell-autonomous role in the transport of GLR-1. CaMKII can have non-catalytic activity in addition to its well-known kinase function (Bingol et al., 2010). To distinguish between these roles, we measured GLR-1 flux in transgenic *unc-43(lf)* mutants that expressed an engineered "kinase-dead" variant of UNC-43 either alone (K42R) or in combination with a second mutation that partially eliminates CaMKII's dependence on Ca^{2+} (K42R; T286D) (Rongo and Kaplan, 1999). Neither variant rescued GLR-1 flux, leading us to conclude that UNC-43/CaMKII kinase activity was required for transport (Figures 2A and 2B).

We considered that the transport defects observed in *unc-43* mutants might be a consequence of more general defects in motor-mediated transport. To address this possibility, we first examined the movement of UNC-116/KIF5 tagged with GFP and did not observe any defects in movement (Figure S2A). We also measured the rate of fluorescence recovery after photobleaching (FRAP) of UNC-116::GFP and found no difference between *unc-43(lf)* and wild-type (Figure S2B). Furthermore, microtubule polymerization in AVA appeared normal in *unc-43(lf)* mutants (Figure S2C). Finally, we asked whether all UNC-116/KIF5-mediated cargo transport was dependent on UNC-43/CaMKII by examining the movement of VAMP/synaptobrevin,

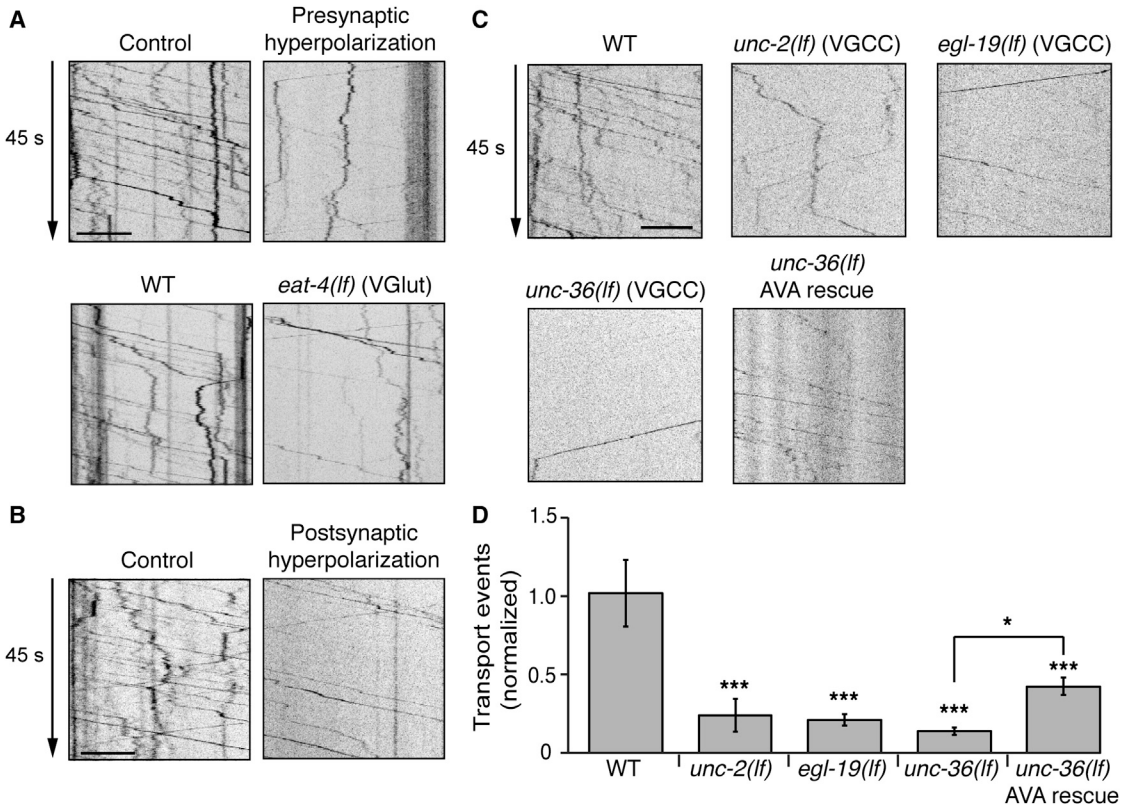

Figure 1. Neuronal Activity and Voltage-Gated Calcium Channels Are Required for GLR-1 Transport

(A) Top row: kymographs of GLR-1::GFP transport in non-transgenic (Control) and transgenic (Presynaptic hyperpolarization) worms that expressed *Peat-4::HisCl1* in presynaptic glutamatergic neurons. Both were treated with 10 mM $HisCl_2$. Bottom row: GLR-1::GFP transport in wild-type (WT) and *eat-4(lf)* mutants.

(B) GLR-1::GFP transport in non-transgenic (Control) and transgenic worms that expressed *Pflp-18::HisCl1* in the AVA neurons (Postsynaptic hyperpolarization). Both worms were treated with 10 mM $HisCl_2$.

(C) SEP::mCherry::GLR-1 transport (mCherry fluorescence) in WT worms and VGCC mutants *egl-19(n582)*, *unc-2(ox2)*, *unc-36(e251)* and a transgenic *unc-36* mutant that expressed a wild-type *unc-36* transgene in AVA (AVA rescue).

(D) The total number of transport events (anterograde and retrograde) normalized to WT, n > 6 for each condition. *p < 0.05, **p < 0.01, ***p < 0.001.

Scale bars represent 5 μm. Error bars indicate SEM. See also Figure S1.

a synaptic vesicle protein previously identified to be an UNC-116/KIF5 cargo (Byrd et al., 2001). We confirmed that VAMP transport was defective in *unc-116* mutants but found no obvious defects in *unc-43(lf)* mutants (Figure S2D).

To determine whether CaMKII has an evolutionarily conserved function with respect to AMPAR transport, we expressed a vertebrate (mouse) alpha-CaMKII (mCaMKII) specifically in the AVA neurons of *C. elegans unc-43(lf)* transgenic mutants and found that this partially rescued GLR-1 transport defects (Figures 2A and 2B). This result indicated that mCaMKII phosphorylated the relevant *C. elegans* substrates and played a conserved role in regulating AMPAR transport.

Glutamate-Gated Current Is Greatly Diminished in *unc-43(lf)* Mutants

We next asked whether the defects in AMPAR flux were associated with a change in glutamate-gated current. Voltage-clamp records from AVA revealed that peak current in response to pressure application of glutamate (Figure S1A) was dramatically decreased in *unc-43(lf)* mutants (Figures 2C and 2D). Current amplitude was rescued by cell-specific expression of either wild-type UNC-43 or mouse CaMKII, indicating a cell-autonomous and evolutionarily conserved role for CaMKII in the regulation of AMPARs (Figures 2C and 2D).

Pressure application of glutamate activates both synaptic and extrasynaptic pools of AMPARs in the AVA neural process. To determine whether synaptic currents were modified in *unc-43(lf)* mutants, we measured endogenous synaptic activity in wild-type and *unc-43(lf)* worms and found that mEPSC amplitude was significantly reduced in *unc-43* mutants (Figures 2E and 2F). Furthermore, we found no appreciable difference in acetylcholine (ACh)-gated currents between wild-type and *unc-43(lf)* mutants (Figures S3A and S3B), indicating that CaMKII has some specificity with respect to the regulation of ligand-gated receptors.

UNC-43/CaMKII Functions Downstream of VGCCs and Upstream of Kinesin-1 Motors

To further characterize the signaling pathway that regulates GLR-1 transport, we examined transport in *unc-43* mutants

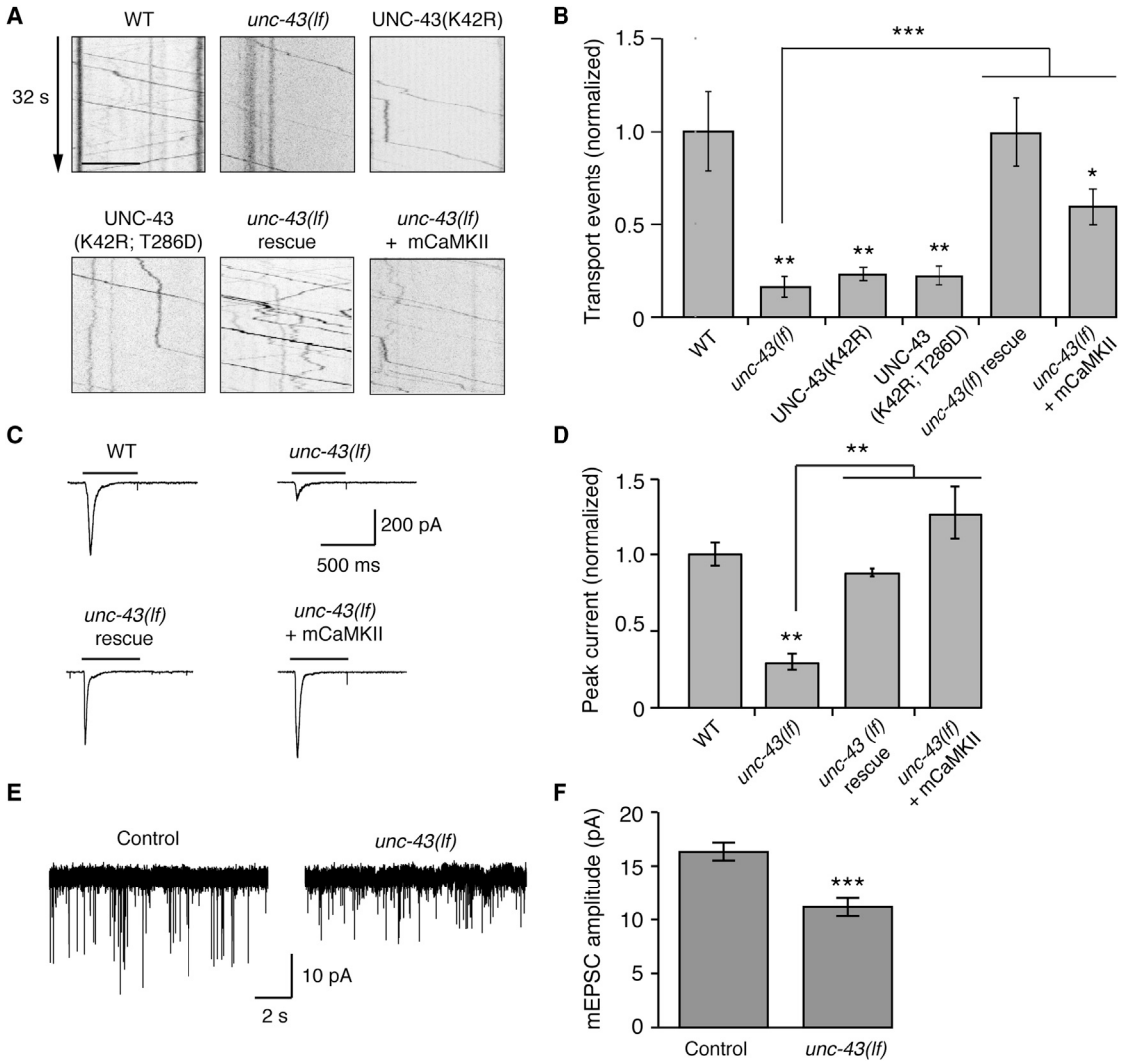

Figure 2. Transport and GLR-1-Mediated Currents Depend on UNC-43/CaMKII Function

(A) GLR-1::GFP transport in WT, an *unc-43(n498n186)* loss-of-function *(lf)* mutant, and transgenic mutants that expressed a wild-type *unc-43* transgene (*unc-43(lf)* rescue), the mouse alpha-CaMKII (*unc-43(lf)* + mCaMKII), or UNC-43 variants with mutations in the kinase domain (K42R) or in the kinase and autophosphorylation domains (K42R; T286D). Scale bar represents 5 μm.

(B) The total number of transport events normalized to WT. n > 7 for each condition.

(C) Glutamate-gated currents in AVA. All worms expressed GLR-1::GFP in AVA.

(D) Peak glutamate-gated current normalized to WT. n > 5 for each condition.

(E and F) Ionotropic glutamate receptor-mediated mEPSCs (E) and the average peak mEPSC amplitude (F) in the AVA neurons of wild-type (Control) and *unc-43(lf)* mutants. n > 100 mEPSC per genotype.

Significantly different from WT, *p < 0.05, **p < 0.01, ***p < 0.001. Error bars indicate SEM. See also Figures S2 and S3.

with a gain-of-function (*gf*) point mutation (*n498sd*) that modifies the kinase such that its function is partially independent of Ca^{2+} (Reiner et al., 1999). In these mutants, GLR-1 flux was significantly greater than in wild-type and neither presynaptic nor postsynaptic HisCl1-mediated hyperpolarization decreased the flux (Figures 3A–3D). To directly test whether the effects of *unc-43(gf)* on AMPAR flux were independent of VGCCs, we examined flux in *unc-36(lf); unc-43(gf)* double mutants. In contrast to the greatly diminished flux in *unc-36(lf)* single mutants (Figure 1D), flux in the double mutants was approximately the same as in the *unc-43(gf)* single mutants (Figures 3E and 3F). The results of this epistasis analysis are consistent with CaMKII functioning downstream of VGCCs in the control of AMPAR flux.

We found extensive co-localization of GLR-1, UNC-43/CaMKII, and UNC-116/KIF5 in the AVA cell body and processes (Figures S4A and S4B). In *unc-43(lf)* mutants, AMPAR flux is greatly decreased despite UNC-116/KIF5 motors moving along apparently normal microtubules (Figure S2C). These results are consistent with either UNC-43/CaMKII acting upstream of UNC-116/KIF5 to promote AMPAR flux or UNC-116/KIF5 acting

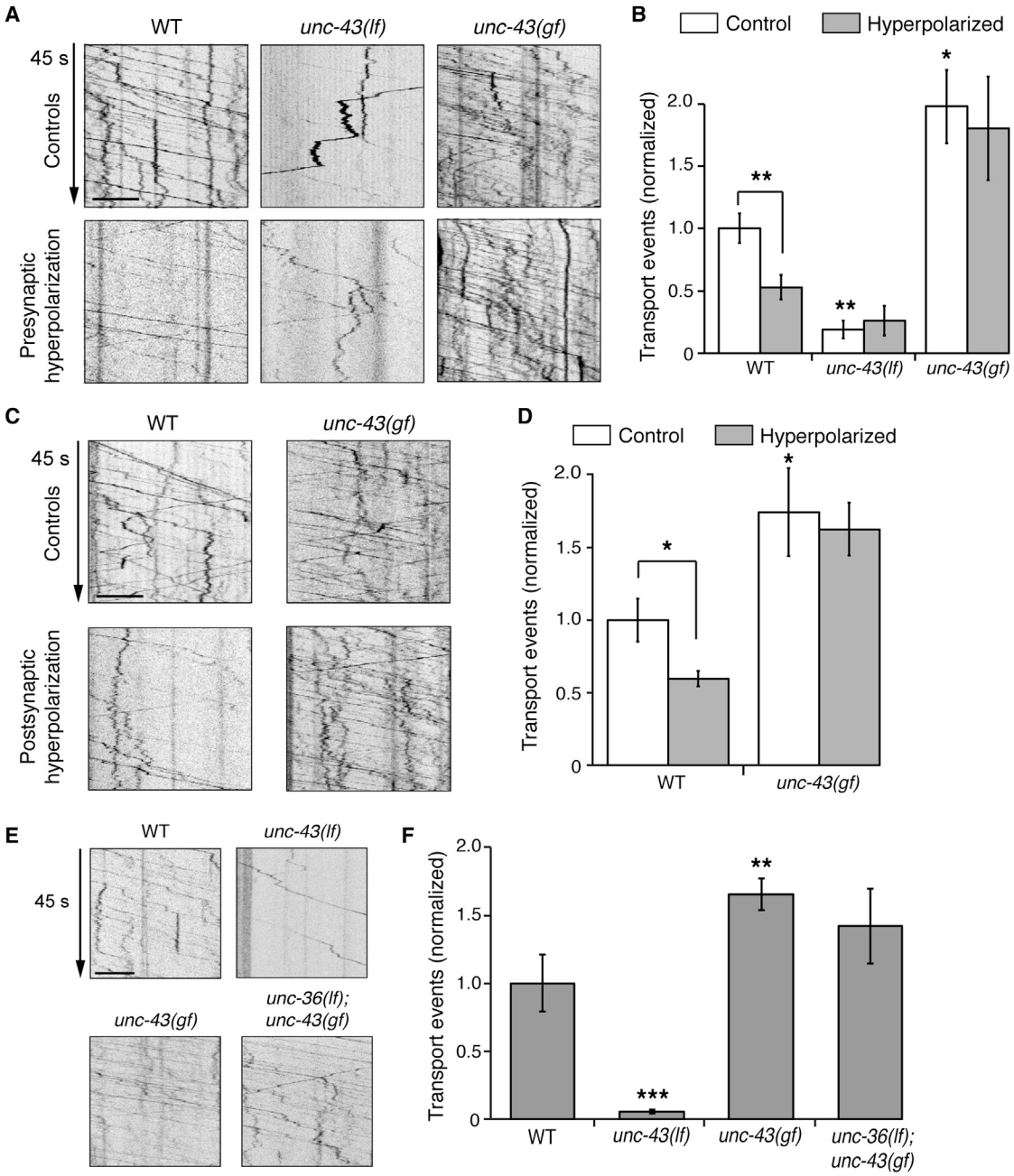

Figure 3. The Regulation of GLR-1 Transport by Neuronal Activity Depends on UNC-43/CaMKII

(A and B) GLR-1::GFP transport in non-transgenic WT, *unc-43(lf)*, and *unc-43(n498sd)* gain-of-function *(gf)* mutants (Controls), and transgenic worms that expressed *Peat-4::HisCl1* in glutamatergic neurons (Presynaptic hyperpolarization). All worms were treated with 10 mM $HisCl_2$. (B) The total number of transport events normalized to WT control. n > 8 for each condition.

(C) GLR-1::GFP transport in non-transgenic (Controls) and transgenic worms that expressed *Pflp-18::HisCl1* in the AVA neurons (Postsynaptic hyperpolarization). All worms were treated with 10 mM $HisCl_2$.

(D) The total number of transport events normalized to WT control. n > 5 for each condition.

(E) SEP::mCherry::GLR-1 transport (mCherry fluorescence) in WT and various single and double mutants.

(F) The total number of transport events normalized to WT. n > 5 for each condition.

*p < 0.05, **p < 0.01, ***p < 0.001. Scale bars represent 5 μm. Error bars indicate SEM.

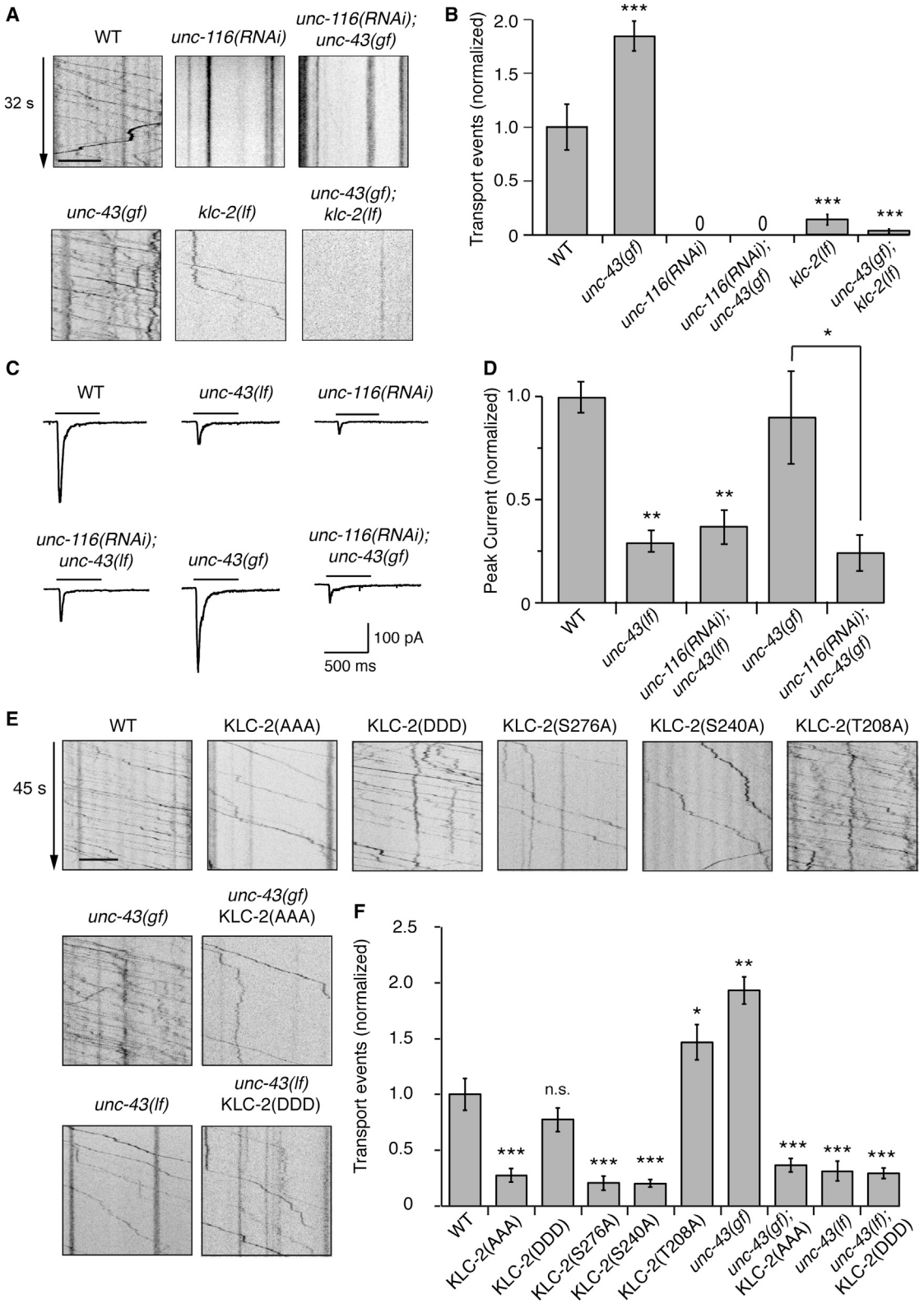

(legend on next page)

in a regulatory step upstream of UNC-43/CaMKII. To distinguish between these models, we generated double mutants between *unc-43(gf)*, which has greater than normal AMPAR flux, and *unc-116(RNAi)*. In a previous study, we found that GLR-1 flux in the AVA neurons was greatly reduced by cell-specific *RNAi* knockdown of *unc-116* in AVA (Hoerndli et al., 2013). We found that flux in *unc-116(RNAi); unc-43(gf)* double mutants was indistinguishable from that of *unc-116(RNAi)* single mutants (Figures 4A and 4B). Importantly, UNC-43/CaMKII was still found at synapses in *unc-116(lf)* mutants (Figure S4C).

In an independent test, we examined flux in double mutants between *unc-43(gf)* and kinesin light chain 2 (*klc-2*). In *klc-2* single mutants, AMPAR flux is dramatically reduced (Figures 4A and 4B) (Hoerndli et al., 2013) and AMPAR-mediated currents decreased (data not shown). Similar to *unc-116(RNAi)* knockdown, *klc-2(lf)* suppressed the increased flux observed in *unc-43(gf)* with *unc-43(gf); klc-2(lf)* double mutants showing similar defects to *klc-2(lf)* single mutants (Figures 4A and 4B). Additionally, KLC-2 co-localized with GLR-1 in AVA processes (Figure S5A). These results are consistent with AMPAR flux being dependent on an UNC-116–KLC-2 motor complex that functions downstream of UNC-43/CaMKII.

Consistent with the effects on AMPAR flux, we found that current amplitudes in *unc-43*(*lf*) were approximately the same as those in *unc-116(RNAi)* mutants and indistinguishable from *unc-116(RNAi); unc-43(lf)* double mutants (Figures 4C and 4D). Furthermore, current amplitudes in *unc-116(RNAi); unc-43(gf)* were approximately the same magnitude as those in *unc-116(RNAi)*, providing additional support for the notion that UNC-43/CaMKII acts upstream of UNC-116/KIF5 (Figures 4C and 4D).

To gain additional mechanistic insight into this signaling pathway, we sought to identify potential targets of CaMKII. It is well known that AMPARs can be phosphorylated by CaMKII (Hell, 2014); however, the extent of this phosphorylation and importance for cellular processes such as LTP has recently been questioned (Granger et al., 2013; Hosokawa et al., 2015). Using multiple algorithms, we were unable to identify consensus CaMKII phosphorylation sites in the primary amino sequence of GLR-1. Additionally, a line-up of the amino acid sequence of mammalian GluA1 and *C. elegans* GLR-1 did not identify a site in GLR-1 that is equivalent to the GluA1 S831 CaMKII phosphorylation site.

We also searched for possible consensus CaMKII phosphorylation sites in motor proteins and found three strong consensus sites in KLC-2 (T208, S240, and S276). We mutated all three sites to alanine (A) residues and expressed the modified protein, KLC-2(AAA), in transgenic worms. The mutations did not decrease the expression of KLC-2 (Figure S5B) but did dramatically reduce AMPAR flux (Figures 4E and 4F). Importantly, KLC-2(AAA) reduced flux in *unc-43(gf)* mutants, a finding that supports the notion that UNC-43/CaMKII functions upstream of the motor complex.

We extended our analysis by evaluating single point mutations and observed decreased AMPAR flux with S276A and S240A, but not T208A, in which flux was somewhat increased (Figures 4E and 4F). We also evaluated flux in transgenic worms that expressed a phosphomimetic form of KLC-2 (where all three sites were mutated to D residues) and found that transport was indistinguishable from wild-type (Figures 4E and 4F). Importantly, KLC-2(DDD) did not restore AMPAR transport in *unc-43(lf)* mutants (Figures 4E and 4F). This finding indicates that CaMKII has additional targets that contribute to AMPAR transport. Together, our results are consistent with a model where UNC-43/CaMKII functions downstream of VGCCs and upstream of UNC-116 and KLC-2 to regulate AMPAR transport.

The Abundance of Synaptic AMPARs Is Altered in *unc-43(lf)* Mutants

In *unc-116/KIF5* mutants, GLR-1 receptors can slowly diffuse to synapses in the ventral nerve cord, where they accumulate as a consequence of defective removal (Hoerndli et al., 2013). To determine whether GLR-1 also accumulates at synapses in *unc-43* mutants, we inserted pH-sensitive superecliptic pHluorin (SEP) and mCherry in tandem at the extracellular N-terminal domain of GLR-1 (Hoerndli et al., 2013; Kennedy and Ehlers, 2011) and expressed this functional fusion protein in the AVA neurons of transgenic wild-type and mutant worms. Similar to *unc-116* mutants, we observed an increase in SEP fluorescence in *unc-43(lf)* mutants compared to wild-type worms (Figure S6A). Cell-specific expression of a wild-type *unc-43* transgene in AVA rescued the SEP fluorescence phenotype (*unc-43(lf)* rescue; Figure S6A). Importantly, GLR-1 also accumulated in the region of the nerve ring where we pressure applied glutamate (Figure S1A).

While synaptic GLR-1 is increased in *unc-116/KIF5* mutants, synaptic levels of the GLR-2 subunit are reduced (Hoerndli et al., 2013). In the absence of UNC-116/KIF5 motor-driven transport GLR-2 is degraded, resulting in fewer GLR-1/GLR-2 heteromeric receptors at synapses, and consequently a decrease in glutamate-gated current (Hoerndli et al., 2013). We found that synaptic GLR-2 was similarly decreased in *unc-43(lf)* mutants (Figure S6B). Thus, with respect to the transport of GLR-1 and GLR-2, and their abundance at synapses,

Figure 4. UNC-43/CaMKII Functions Upstream of UNC-116/KIF5 and KLC-2 to Regulate AMPAR Transport

(A) GLR-1::GFP transport in WT, *unc-116(RNAi)*, *unc-43(gf)*, and *klc-2(km11)* loss-of-function *(lf)* single and double mutants.

(B) The total number of transport events normalized to WT. No events were detected in *unc-116(RNAi)* or *unc-116(RNAi); unc-43(gf)* mutants. n = 8 for each condition.

(C) Glutamate-gated currents in the AVA neurons of transgenic worms that expressed GLR-1::GFP in AVA.

(D) Peak glutamate-gated current normalized to WT. n > 5 for each condition.

(E) GLR-1::GFP transport in WT and transgenic worms that expressed a KLC-2 variant with a single point mutation, KLC-2(S276A), KLC-2(S240A), or KLC-2(T208A), or a variant with three point mutations, KLC-2(AAA) or KLC-2(DDD), in potential UNC-43/CaMKII phosphorylation sites. All KLC-2 variants were tagged with tagRFP-T.

(F) The total number of transport events normalized to WT. Significance tested by one-way ANOVA with Tukey's multiple comparison.

*p < 0.05, **p < 0.01, ***p < 0.001. Error bars indicate SEM. Scale bars represent 5 μm. See also Figures S4, S5, and S6.

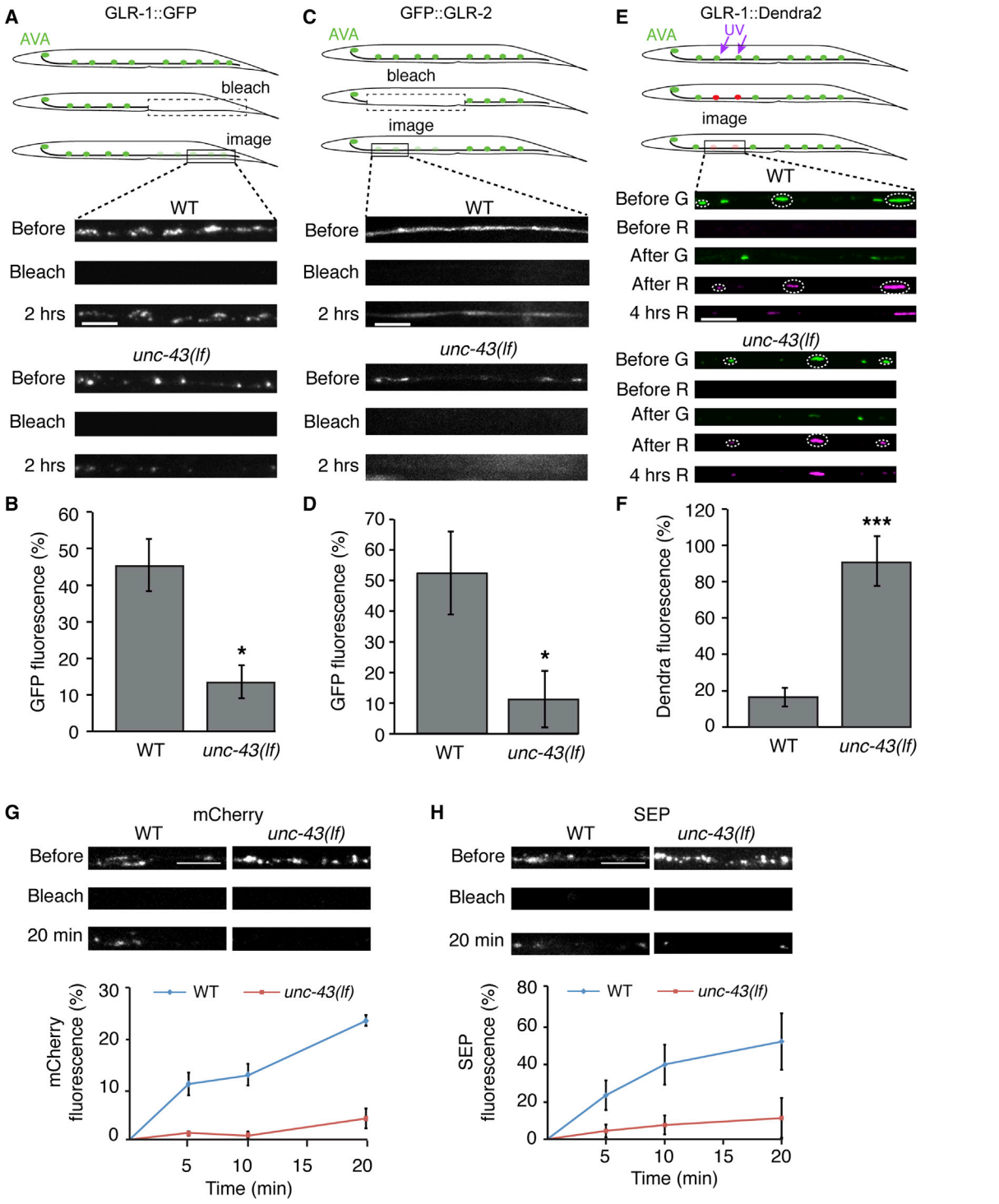

Figure 5. Synaptic Delivery, Removal, and Insertion of GLR-1 Are Disrupted in *unc-43(lf)* Mutants

(A) Confocal images of GLR-1::GFP in the distal region of AVA taken before, immediately after and 2 hr after photobleaching GLR-1::GFP.

(B) GLR-1::GFP puncta fluorescence 2 hr after photobleaching as a percentage of the pre-bleach signal. n > 6 worms per condition.

(C) Confocal images of GFP::GLR-2 in the proximal region of AVA taken before, immediately after and 2 hr after photobleaching GFP::GLR-2.

(D) GFP::GLR-2 puncta fluorescence 2 hr after photobleaching as a percentage of the pre-bleach signal. n > 4 worms per condition.

(E) Confocal images of GLR-1::Dendra2 in the proximal region of AVA. Shown are green (G) and red (R) fluorescence before, immediately after or 4 hr after photoconversion. White dashed circles indicate GLR-1 synaptic puncta targeted for conversion.

(legend continued on next page)

unc-43 and *unc-116* mutants have nearly identical phenotypes, suggesting a common signaling pathway. Our finding that GLR-1, UNC-116, and UNC-43 co-localize in the cell body and at synapses also supports this hypothesis (Figures S4A and S4B).

In *unc-43* mutants, GLR-1 accumulates at synapses, presumably by diffusion. In contrast, GLR-2 is degraded in the absence of motor-driven transport (Hoerndli et al., 2013) and is lacking at synapses in *unc-43* mutants (Figure S6B). Thus, the decreased currents in *unc-43* mutants (Figure 2C) might be secondary to limited amounts of synaptic GLR-2. In support of this model, we found that the peak amplitude of glutamate-gated current was quite similar in *unc-43* and *glr-2* mutants (Figure 4C; Figure S6C). Additional support comes from our finding that the current in *glr-2; unc-43* double mutants was not appreciably different than that measured from either single mutant. Importantly, we found that the glutamate-gated current recorded from transgenic *glr-2; unc-43* double mutants that overexpressed GLR-2 was rescued to wild-type levels (*glr-2(lf); unc-43(lf)* + GLR-2; Figure S6C).

Delivery and Removal of Synaptic AMPARs Are Reduced in *unc-43* Mutants

To more directly measure the effects of UNC-43/CaMKII on the delivery of synaptic GLR-1 and GLR-2, we measured FRAP of GFP-tagged GLR-1 or GLR-2 in the AVA processes. In wild-type worms, half-recovery of the fluorescent signal occurred within 2 hr after photobleaching (Figures 5A–5D). In contrast, recovery was much slower in *unc-43(lf)* mutants, consistent with the measured defects in AMPAR flux.

Our finding that GLR-1 accumulated at synapses in *unc-43(lf)* mutants (Figure S6A) suggested that UNC-43/CaMKII is required for synaptic removal of GLR-1. To measure the removal rate, we expressed GLR-1 tagged with the photo-convertible fluorophore Dendra2 in transgenic wild-type and mutant worms (Gurskaya et al., 2006). Using local illumination with UV light, we converted synaptic GLR-1::Dendra2 from green to red fluorescence and measured the subsequent loss of red fluorescence. We found that the decay of red fluorescence was greatly slowed in *unc-43(lf)* mutants when compared to wild-type (Figures 5E and 5F), a result consistent with the electrophysiological data. The decreased rate of removal was similar to that previously described for *unc-116* mutants (Hoerndli et al., 2013).

To distinguish surface from intracellular receptors, we expressed SEP::mCherry::GLR-1 in transgenic worms and simultaneously measured the rate of synaptic delivery of GLR-1 and the rate of GLR-1 insertion in the cell membrane following photobleaching of both fluorophores. Bleaching eliminates mCherry fluorescence from both intracellular receptors and those inserted in the membrane; but only SEP fluorescence from surface receptors can be bleached because SEP in acidic endocytic vesicles is resistant to photobleaching (Sankaranarayanan et al., 2000). We found that the recovery of membrane GLR-1 (SEP fluorescence) and the delivery of GLR-1 to synapses (mCherry fluorescence) were dramatically decreased in *unc-43(lf)* mutants (Figures 5G and 5H).

Interestingly, we noted that in wild-type animals the initial rate of SEP recovery was faster than that of mCherry. For single synaptic puncta, the ratio of SEP to mCherry fluorescence in wild-type worms was significantly larger 5 min after photobleaching compared to the ratio before bleaching (Figures S7A and S7B). This result suggests that the endosomal population of receptors, which are resistant to SEP photobleaching, is the primary source of new surface receptors immediately following photobleaching. The different rates of recovery of SEP and mCherry fluorescence indicate that initial GLR-1 surface recovery is not tightly linked to the kinesin-mediated delivery of new receptors to the endosome. This observation, using dual FRAP, is consistent with our previous measurements of the in vivo transport of SEP::mCherry::GLR-1 (Hoerndli et al., 2013) and suggests differential rates of local recycling of receptors and delivery of new receptors by the kinesin motor UNC-116/KIF5.

Localized Inactivation of UNC-43/CaMKII Reveals Its Essential Role in the Cellular Export of AMPARs

Our results demonstrate that UNC-43/CaMKII has at least three roles with respect to GLR-1 AMPARs. It is required for motor-driven delivery and removal of synaptic GLR-1, as well as the membrane insertion of GLR-1. The defective transport of GLR-1 could reflect a critical role for UNC-43/CaMKII in the initial loading of GLR-1 cargo onto motors, or it could indicate that the continued association between GLR-1 cargo and the motor requires the continued presence (co-transport) of UNC-43/CaMKII. To distinguish between these possibilities, we acutely inactivated UNC-43/CaMKII using the recently described technique of chromophore-assisted light inactivation (CALI) (Lin et al., 2013; Shu et al., 2011). We generated transgenic *unc-43(lf)* and *unc-116(lf)* mutants that expressed a functional miniSOG::UNC-43 or UNC-116::miniSOG fusion protein, respectively. MiniSOG (mini-singlet oxygen generator) is a 106 amino acid, genetically encoded fluorescent flavoprotein that functions as a photosensitizer. Illumination with blue light leads to inactivation of proteins within a small radius (~70 nm) allowing for temporal and spatial control of protein inactivation (Lin et al., 2013; Shu et al., 2011).

To test the hypothesis that UNC-43/CaMKII is required either directly or indirectly for loading of GLR-1 cargo onto molecular motors, or for the exit of motor-driven cargo from the cell body, we used CALI to selectively inactivate miniSOG::UNC-43 in the cell body (see Experimental Procedures), while imaging transport of GLR-1::mCherry in the proximal region of the AVA processes. Following CALI, anterograde transport of GLR-1

(F) Quantification of the red fluorescent signal remaining 4 hr after photoconversion as a percentage of that immediately after photoconversion. n > 10 puncta per genotype.

(G and H) Confocal images and FRAP quantification of either mCherry (G) or SEP (H) in transgenic worms that expressed SEP::mCherry::GLR-1 in AVA. Images were taken before, immediately after, and 20 min after photobleaching. n = 5 worms per genotype. SEP and mCherry FRAP in *unc-43(lf)* was significantly different from WT, $p < 0.001$ and $p < 0.01$, respectively (ANCOVA analysis).

Significantly different from WT, *$p < 0.05$; ***$p < 0.001$. Scale bars represent 5 μm. Error bars indicate SEM. See also Figure S7.

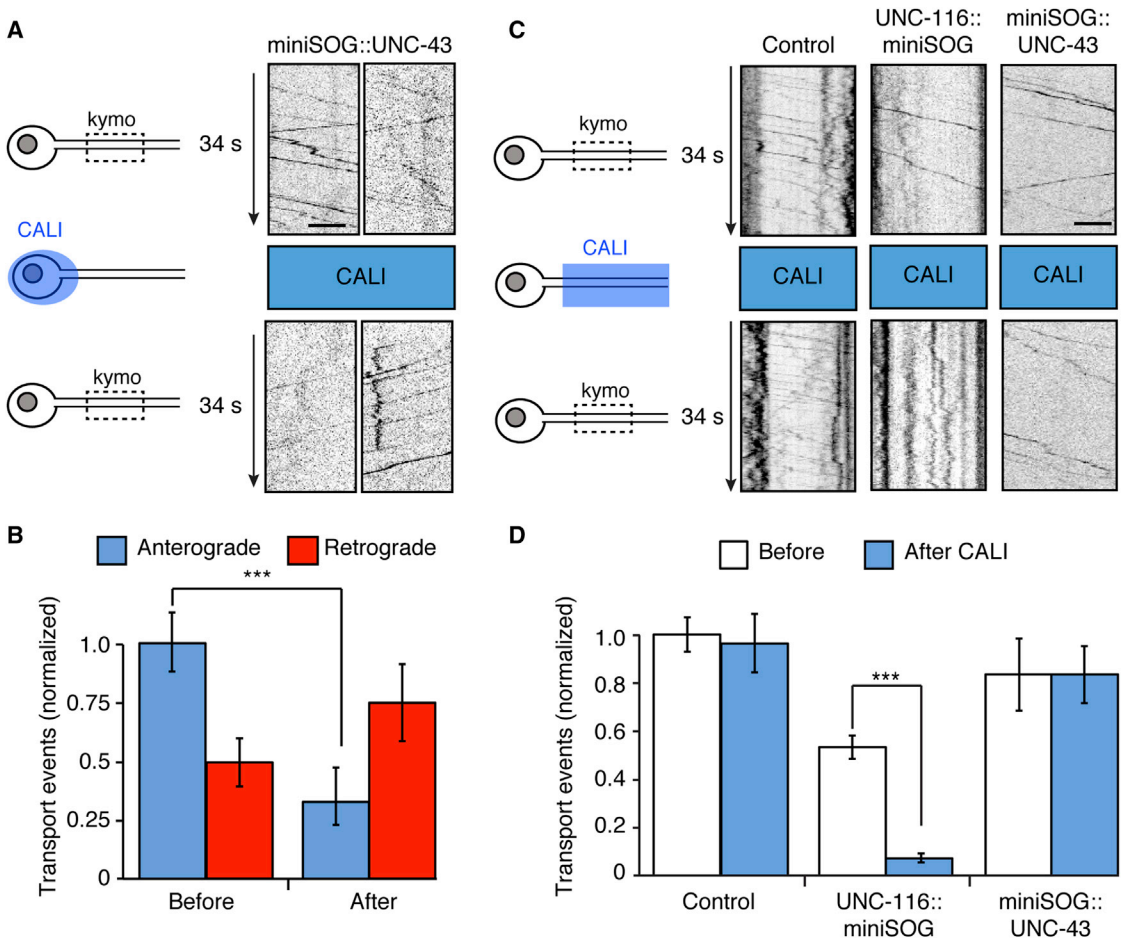

Figure 6. UNC-43/CaMKII Function in the Cell Body Is Critical for GLR-1 Transport

(A) Two examples of GLR-1::mCherry transport in transgenic *unc-43(lf)* mutants that expressed miniSOG::UNC-43 in AVA. Shown is transport before (top) and 4 min after (below) blue-light inactivation (CALI) of miniSOG::UNC-43 in the cell body.

(B) Quantification of anterograde and retrograde transport events following miniSOG::UNC-43 inactivation in the cell body. n = 11 worms per condition.

(C) GLR-1::GFP transport in WT and transgenic *unc-116(lf)* and *unc-43(lf)* mutants that expressed UNC-116::miniSOG and miniSOG::UNC-43, respectively. Shown are images before and after CALI.

(D) The total number of transport events before and after CALI. n = 4 worms per condition.

***p < 0.001. Error bars indicate SEM. See also Figure S7.

was greatly diminished, with no apparent effect on retrograde transport from distal regions that did not receive CALI (Figures 6A and 6B). These results are consistent with UNC-43/CaMKII promoting the loading of GLR-1 cargo onto UNC-116 (kinesin-1) motors at the cell body or the initial portion of the AVA process. They also suggest that UNC-43/CaMKII might have a similar role in the loading of GLR-1 at synapses because we observed defective removal of GLR-1::Dendra2 in *unc-43(lf)* mutants (Figures 5E and 5F).

We also used CALI to selectively inactivate either UNC-116/KIF5 or UNC-43/CaMKII in the proximal processes of the AVA neurons. Following CALI, we monitored GLR-1 transport in the same region. Compared to wild-type controls, we observed diminished GLR-1 flux following CALI in worms that expressed UNC-116::miniSOG (Figures 6C and 6D). In experiments that combined CALI of UNC-116 with photobleaching of SEP::mCherry::GLR-1 in the proximal processes of AVA, FRAP of mCherry, but not SEP, was slowed (Figure S7C). This result is consistent with decreased GLR-1 transport along the region of the processes where UNC-116 was inactivated; but perhaps because UNC-43/CaMKII is still found at synapses in *unc-116* mutants, receptors already at endosomal compartments can translocate to the cell membrane (Figure S4C). In contrast, we observed no significant decrease in GLR-1 flux following CALI of miniSOG::UNC-43 in the AVA processes, indicating that UNC-43/CaMKII is not required for transporting GLR-1 cargo that is already loaded on motors (Figures 6C and 6D). Finally, we did not observe co-transport of UNC-43 and GLR-1 in transgenic worms that expressed both mCherry::UNC-43 and GLR-1::GFP in AVA (Figure S7D), a finding consistent with the results of CALI of miniSOG::UNC-43 in the processes of AVA.

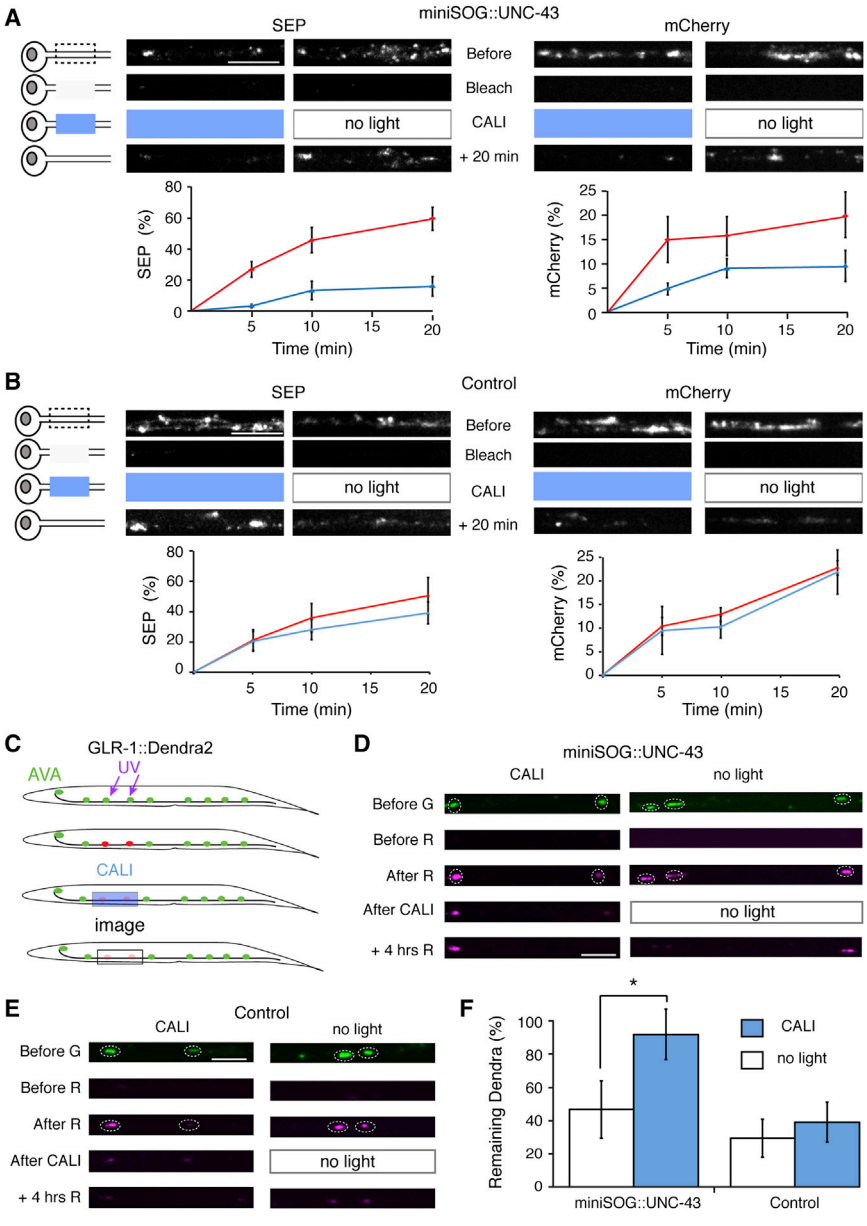

Figure 7. UNC-43/CaMKII Is Required for GLR-1 Insertion and Removal at Synapses

(A and B) Confocal images of SEP::mCherry::GLR-1 in transgenic *unc-43(lf)* mutants that expressed miniSOG::UNC-43 in AVA (A), and non-transgenic wild-type worms (Control) (B). SEP and mCherry FRAP in transgenic worms exposed to blue light (CALI) was significantly different from transgenic worms without light exposure, $n > 5$ per condition, $p < 0.01$ (ANCOVA analysis). FRAP in control worms exposed to blue light was not significantly different from no light controls.

(C–E) Schematic (C) and confocal images (D and E) of GLR-1::Dendra2 photoconversion in proximal AVA synapses followed by CALI inactivation of miniSOG::UNC-43 in either transgenic *unc-43(lf)* mutants (D) or non-transgenic controls (E).

(F) Quantification of the red fluorescent signal remaining 4 hr after CALI as a percentage of that immediately after CALI. $n = 5$, worms per condition. $^*p < 0.05$.

Scale bars represent 5 μm. Error bars indicate SEM.

miniSOG::UNC-43 in the same region, making sure to avoid the cell body. We then simultaneously monitored the recovery of both SEP and mCherry fluorescence. We found that membrane insertion of GLR-1 was greatly diminished following CALI as indicated by the slower rate of SEP FRAP compared to no light controls (Figure 7A). Furthermore, we found that mCherry recovery was also diminished following local CALI inactivation of miniSOG::UNC-43 when compared to controls (Figure 7A). In additional control experiments, we found no effect of light illumination alone in worms that did not express miniSOG::UNC-43 (Figure 7B). These results indicate that synaptically localized UNC-43/CaMKII has an ongoing role to promote the membrane insertion of GLR-1 and is also required for the local capture of transported GLR-1 cargo at synapses.

UNC-43/CaMKII Is Required at Synapses for Surface Delivery of AMPARs

Following photobleaching of surface GLR-1 receptors (SEP fluorescence), we found that fluorescence recovery was slower in *unc-43(lf)* mutants than in wild-type, despite the presence of synaptically localized, subcellular accumulations of GLR-1 (mCherry fluorescence; Figure S6B). The defective insertion of synaptic GLR-1 receptors in *unc-43(lf)* mutants might be due to a loss of CaMKII function at synapses. Alternatively, UNC-43/CaMKII might be required in the cell body for the delivery of an additional protein(s) required for membrane insertion of GLR-1.

To distinguish between these two models of UNC-43/CaMKII function, we first photobleached SEP::mCherry::GLR-1 along the AVA processes and then used CALI to selectively inactivate

UNC-43/CaMKII Is Required at Synapses for the Removal of Synaptic AMPARs

To test whether synaptically localized CaMKII was required for the removal of AMPARs, we photoconverted GLR-1::Dendra2 (from green to red fluorescence) in the process of AVA (Figure 7C). Following photoconversion, we again used CALI to selectively inactivate miniSOG::UNC-43 in the same region. We then monitored the loss of Dendra2 red fluorescence. We found that synaptic red fluorescence was more stable following CALI inactivation of miniSOG::UNC-43 compared to controls (Figures 7D–7F), a finding that is consistent with a slower rate of GLR-1 removal in *unc-43(lf)* mutants (Figures 5E and 5F).

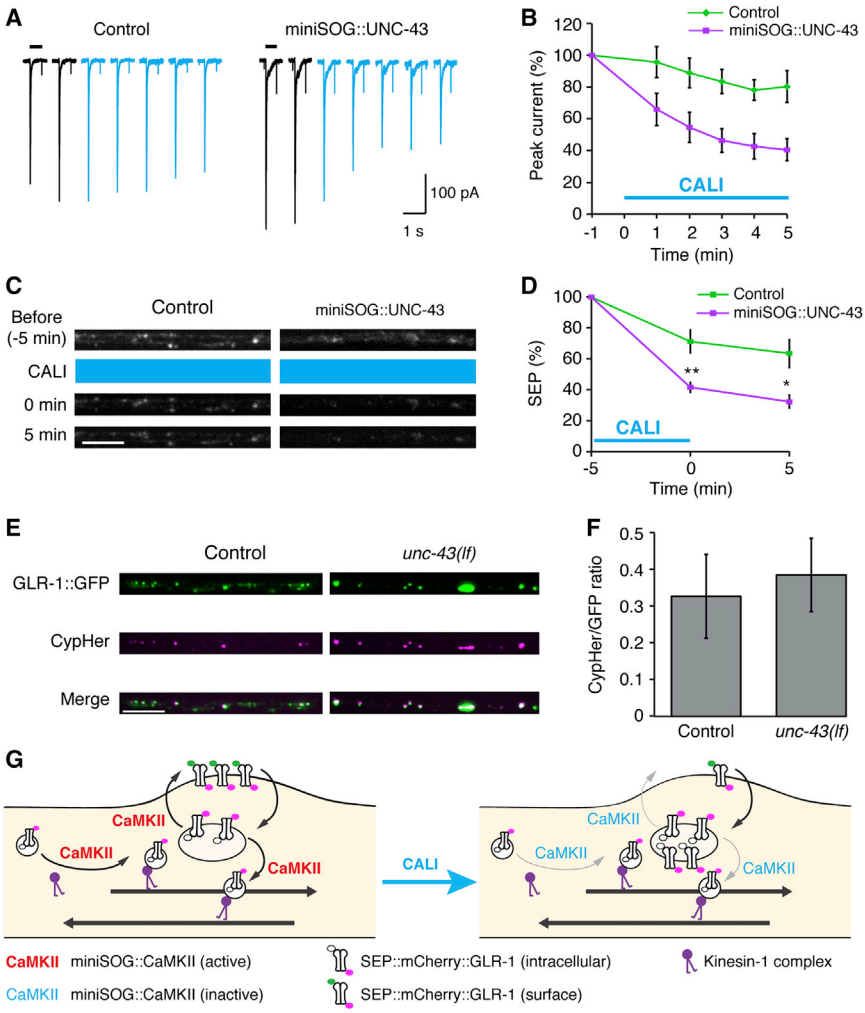

Figure 8. Acute Inactivation of UNC-43/CaMKII in Adult Worms Reduced Glutamate-Gated Current

(A) Glutamate-gated currents in AVA before (black) and after (blue) CALI in wild-type worms or transgenic *unc-43(lf)* mutants that expressed miniSOG::UNC-43. Currents were measured at 1-min intervals.

(B) Peak glutamate-gated current normalized to the average peak current before CALI treatment. n > 6 per condition. Current decrease in transgenic worms was significantly different than in wild-type controls, $p < 0.01$ (ANCOVA analysis).

(C) Confocal images of SEP fluorescence in transgenic wild-type worms (Control) that expressed SEP::mCherry::GLR-1 and transgenic *unc-43(lf)* mutants that also expressed miniSOG::UNC-43 in AVA.

(D) Quantification of SEP fluorescence after CALI as a percentage of the fluorescence before CALI. n = 6 worms per genotype. *$p < 0.05$, **$p < 0.01$ compared to control.

(E) Confocal images of GFP and anti-HA CypHer fluorescence in transgenic wild-type worms (Control) and *unc-43(lf)* mutants that expressed HA::GLR-1::GFP in AVA.

(F) Quantification of the average ratio of CypHer to GFP fluorescence per puncta.

(G) Model for the role of UNC-43/CaMKII in GLR-1 synaptic delivery, insertion, and removal. CaMKII is required for the delivery of GLR-1 to synapses, membrane insertion (exocytosis), and removal from subsynaptic compartments but not receptor endocytosis. Following acute inactivation of miniSOG::UNC-43 (CaMKII) using CALI, only enodocytosis remains leading to the loss of GLR-1 surface receptors and decreased glutamate-gated current.

Scale bars represent 5 μm. Error bars indicate SEM. See also Figures S8 and S9.

Together, our results indicate that UNC-43/CaMKII is required for the coordinated delivery, insertion and removal of synaptic GLR-1.

UNC-43/CaMKII Has an Ongoing Role in the Maintenance of Glutamate-Gated Current

We next addressed the consequences of CALI of UNC-43/CaMKII for GLR-1-mediated current. In voltage-clamp recordings from AVA in transgenic worms that expressed miniSOG::UNC-43, we measured glutamate-gated current before and after inactivation with blue light. We found that the peak glutamate-gated current rapidly decreased following illumination, with no obvious changes in the current kinetics (Figures 8A and 8B), indicating that the number of functional AMPARs was reduced by CALI inactivation of UNC-43/CaMKII. In contrast, we found no appreciable rundown of NMDA-gated current after CALI (Figure S8). We reasoned that stable AMPAR-mediated currents reflect a balance of UNC-43-dependent insertion of AMPARs and UNC-43-independent endocytosis of AMPARs. Following CALI, insertion is decreased, but if endocytosis proceeds normally, then current should run down. To test this model, we measured SEP::GLR-1 in the proximal processes and found that SEP fluorescence decreased rapidly following CALI of miniSOG::UNC-43 in the same region (Figures 8C and 8D), consistent with ongoing endocytosis of SEP::GLR-1. As an additional test, we examined endocytosis using the pH-sensitive dye CypHer (Tatavarty et al., 2013). We found no difference in the CypHer/GFP ratio between wild-type controls and *unc-43* mutants (Figures 8E and 8F). Thus, acute inactivation of UNC-43/CaMKII revealed three essential roles for CaMKII at synapses: motor-dependent delivery of AMPARs, removal of synaptic AMPARs from endosomal compartments, and exocytosis of new synaptic AMPARs into the cell membrane (Figure 8G).

Local ablation of UNC-43/CaMKII in adult worms revealed ongoing roles for CaMKII in the regulated transport of AMPARs. This result prompted us to ask whether the altered synapses in *unc-43* mutants were developmentally fixed. We addressed this question by driving expression of wild-type UNC-43 in adult *unc-43* mutants using heat shock. We found that heat-shock-driven expression in adult mutants rescued AMPAR transport (Figure S9). These data provide additional evidence for CaMKII's ongoing role in regulating AMPARs in the adult nervous system

and raised the question of whether CaMKII contributes to activity-dependent modification of synaptic strength.

UNC-43/CaMKII Is Required for AMPAR-Mediated Synaptic Plasticity

We previously showed that overexpressing the components required to form a functional AMPAR signaling complex (GLR-1 and GLR-2 along with the auxiliary proteins SOL-1, SOL-2, and STG-2) (Hoerndli et al., 2013; Mellem et al., 2002; Walker et al., 2006a, 2006b; Wang et al., 2008, 2012; Zheng et al., 2004) increased the amplitude of glutamate-gated currents recorded from transgenic *unc-116* mutants but not transgenic wild-type worms (Hoerndli et al., 2013). With respect to *unc-43* mutants, we found that overexpressing the complex caused a large increase in current (Figures 9A and 9B). Importantly, as previously found, overexpression of the complex in wild-type worms did not cause an increase in peak current amplitude. Thus, UNC-43/CaMKII activity maintains the number of functional synaptic AMPARs in the face of significant perturbations. We next asked whether other perturbations, such as sustained synaptic activity, modified synapses and if so, whether CaMKII contributed to synaptic plasticity.

To study synaptic plasticity, we used the *mec-3* promoter to drive expression of a channelrhodopsin variant (ChIEF) in the glutamatergic mechanosensory neurons of transgenic worms, including the PLM neurons (Lee et al., 1999; Way and Chalfie, 1989), which provide approximately two to four synaptic inputs to AVA (http://wormweb.org/neuralnet#c=PLM&m=1) (Figure 9C). We chose ChIEF because it has less inactivation during light application than conventional channelrhodopsin (Lin et al., 2009). We co-expressed *Pmec-3::ChIEF* with the synaptic vesicle associated protein VAMP/synaptobrevin tagged with mCherry (*Pmec-3::VAMP::mCherry*) to identify presynaptic regions and SEP::GLR-1 (expressed in AVA) to identify the corresponding postsynaptic regions (Figure 9D). Excitation with blue light (training; see Experimental Procedures for details) increased the SEP::GLR-1 fluorescent signal in the predicted PLM-AVA glutamatergic synapses, but not in neighboring or distal synapses. No increase in fluorescence was measured in *unc-43(lf)* mutants (Figures 9D–9F). We observed similar results when measuring activity-dependent changes in GLR-1::GFP (Figures 9G–9I). These results indicate that the number of inserted GLR-1 receptors and the total pool of GLR-1 at PLM synapses increased following prolonged stimulation of these synapses and that UNC-43/CaMKII function is required for these changes to occur.

DISCUSSION

Our experiments have revealed that UNC-43/CaMKII has unexpected and fundamentally important roles in the maintenance of synaptic strength. In *unc-43* mutants, transport of AMPARs out of cell bodies is dramatically reduced. This defect was also induced by selective spatiotemporal inactivation of UNC-43/CaMKII in the cell bodies of adult worms and was rescued by heat-shock expression of UNC-43/CaMKII at the adult stage. AMPAR transport was rescued cell autonomously when either UNC-43/CaMKII or mouse alpha-CaMKII was specifically expressed in the AVA neurons. Our FRAP experiments confirmed that synaptic delivery of GLR-1 homomeric and GLR-1/GLR-2 heteromeric AMPARs was greatly reduced in *unc-43* mutants, and the photoconversion experiments demonstrated that receptor removal was also dramatically reduced. These defects are similar to those observed in *unc-116/KIF5* mutants (Hoerndli et al., 2013) and are consistent with UNC-43/CaMKII having either a direct or indirect role in the loading of AMPAR cargo onto UNC-116/KIF5 kinesin motors, which is critical for the synaptic delivery and removal of AMPARs (Figure 8).

We previously reported a significant increase in synaptic accumulation of GLR-1 homomeric receptors in *unc-116* mutants. Conversely, GLR-1/GLR-2 heteromeric receptors were diminished in these mutants because they were selectively degraded in the absence of motor-driven transport. We found similar changes in the distribution and abundance of AMPARs in *unc-43* mutants. Furthermore, glutamate-gated current was greatly diminished in both *unc-116* and *unc-43* mutants, which is consistent with the current's dependence on GLR-1/GLR-2 heteromeric receptors (Hoerndli et al., 2013; Mellem et al., 2002). In the absence of kinesin- and CaMKII-mediated synaptic delivery and removal, GLR-1 homomeric receptors reach synapses by diffusing along neural processes where they subsequently become trapped. In support of this model, we found that driving diffusion of heteromeric receptors by greatly overexpressing the GLR-2 subunit in transgenic *unc-43* mutants increased synaptic GLR-2 and restored glutamate-gated current to wild-type levels. Interestingly, overexpressing all known components of the AMPAR signaling complex (GLR-1, GLR-2, and the auxiliary proteins) in *unc-43* mutants produced currents much larger than those observed when the same components were overexpressed in wild-type controls. Presumably, the increased current was due to heteromeric receptors diffusing to and accumulating at synapses.

By selectively inactivating UNC-43/CaMKII in the cell body of adult worms, we could decrease AMPAR export from the cell body without affecting transport of receptors that had already entered the neural process. Conversely, selective inactivation in the neural process decreased synaptic removal. Together, these data support a model in which UNC-43/CaMKII has a critical role in the loading of AMPAR cargo onto UNC-116/KIF5 motors in the cell body for motor-driven export, and in loading at synapses for their subsequent removal (Figure 8). In vertebrates, there is some evidence that AMPARs bind to scaffolding proteins that serve as adaptors for cargo transport (Setou et al., 2002). However, the identity of these adaptors has not been resolved in vertebrates (Mao et al., 2010) or in *C. elegans*. Of particular interest is whether adaptors that function at the cell body for the initial loading of AMPARs are different from those at synapses required for the removal of AMPARs.

We also found that the size of mEPSC amplitude was reduced in *unc-43* mutants, consistent with the decrease in synaptic GLR-1/GLR-2 heteromeric receptors. The decrease in mEPSC amplitude was not as great as that observed when measuring current in response to pressure application of glutamate. These differences are not directly comparable because pressure application activates both synaptic and extrasynaptic classes of glutamate receptors, whereas mEPSCs represent current

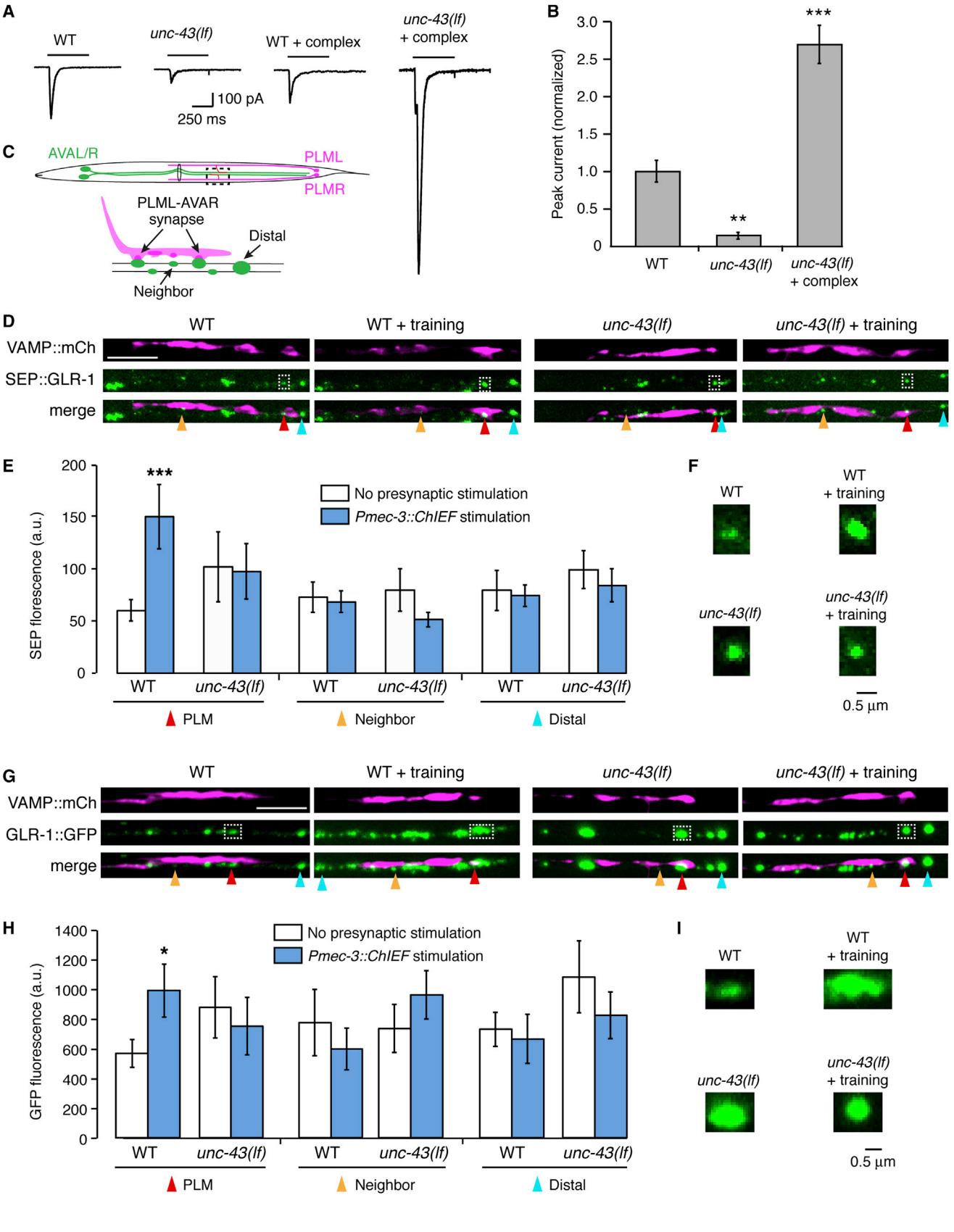

(legend on next page)

mediated by the synaptic population only. Although GLR-1/GLR-2 heteromeric receptors are greatly reduced in *unc-43* mutants, those that do reach synapses by diffusion might preferentially localize to the postsynaptic membrane, perhaps because of greater affinity for the underlying scaffolding machinery, thus explaining the smaller decrease in mEPSC amplitude. Diffusion of receptors is slow and inefficient, but over many days of development receptors can populate distant synapses. What is especially deficient in *unc-43* mutants is the ability to mount rapid changes in receptor number. Our results from FRAP, photoconversion, and plasticity experiments, demonstrated that *unc-43* mutants were deficient in their response to perturbations that required rapid changes in synaptic receptors. Thus, CaMKII is essential for the dynamic control of receptor number at synapses.

UNC-43/CaMKII-Regulated Transport of AMPARs: Implications for Synaptic Plasticity

We demonstrated that overexpressing the GLR-1 signaling complex in transgenic wild-type worms had no effect on the magnitude of the glutamate-gated current, indicating a tight regulation of synaptic and extrasynaptic receptor numbers. In contrast, although currents in *unc-43* mutants are significantly reduced compared to wild-type, the same overexpression perturbation in transgenic mutants resulted in currents that were considerably larger than wild-type. This finding suggests that UNC-43/CaMKII has an important role in the maintenance of synaptic strength by regulating the delivery and removal of synaptic and extrasynaptic receptors.

UNC-43/CaMKII is primarily regulated by intracellular Ca^{2+} (Hell, 2014; Nicoll and Roche, 2013; Shonesy et al., 2014) and thus is responsive to the electrical activity of a neuron. We propose that the overall pattern of VGCC activity, and thus CaMKII activation, regulates kinesin-dependent delivery and removal of AMPARs at neuronal synapses thereby maintaining receptor number, which is a critical factor in the processes of synaptic scaling and homeostasis (Davis, 2006; Goold and Nicoll, 2010; Ibata et al., 2008; Tatavarty et al., 2013; Turrigiano, 2008).

Interestingly, the flux of AMPAR transport vesicles appears to be a readout of synaptic activity. Hyperpolarization of presynaptic inputs or the postsynaptic neuron decreased flux, suggesting that neurons modify AMPAR transport in accordance with the electrical activity of the cell. Thus, to accommodate changes in synaptic activity neurons mobilize an appropriate number of AMPAR transport vesicles. Increased flux along with CaMKII activity at synapses could make rapid changes to synaptic strength because any given synapse is only a few seconds removed from an AMPAR transport vesicle (Hoerndli et al., 2013). Our optogenetic-based plasticity paradigm revealed that synaptic plasticity at glutamatergic synapses is dependent on UNC-43/CaMKII activity. Synaptic activity might initiate a CaMKII-dependent process of AMPAR delivery that is coupled to synaptic insertion of new AMPARs and removal of existing receptors, thus establishing a new level of synaptic strength.

The evolutionarily conserved role of CaMKII in regulating motor-driven AMPAR transport suggests that these processes might be relevant to the phenomena of LTP and LTD in vertebrates. We propose that synaptic signaling resulting in elevated CaMKII activity in the cell body increases the pool of mobile AMPARs available for synaptic delivery. Increased CaMKII activity might also be used to distinguish active synapses from those less active, thus changing the probability of receptor delivery. This mechanism could be self-sustaining and suggests a relatively simple model: the increased number of AMPARs at activity "tagged" or potentiated synapses leads to increases in both Ca^{2+} influx and the probability of CaMKII-mediated AMPAR delivery from mobile pools. This maintains the strength of potentiated synapses leading to long-lived activity-dependent changes in synaptic strength.

Our data suggest that additional unidentified components contribute to the CaMKII regulation of AMPAR transport and the control of synaptic strength. It should be of considerable interest to identify these components as well as the signals that direct cargo to be delivered to or removed from synapses. Our finding that CaMKII is critically important for the regulation of synaptic strength is also relevant to neurodegenerative disorders such as Alzheimer's disease (Huang and Mucke, 2012). Thus, the altered microtubule organization in neurons that is characteristic of Alzheimer's disease might be expected to disrupt kinesin-mediated delivery and removal of synaptic AMPARs, leading to altered synaptic function.

Figure 9. CaMKII/UNC-43 Is Required for Input-Specific Synaptic Plasticity

(A) Glutamate-gated currents in transgenic WT and *unc-43(lf)* mutants that expressed GLR-1::GFP in AVA either with or without overexpression of the GLR-1 signaling complex.

(B) Peak glutamate-gated current normalized to WT. n = 5 for all genotypes, $^{**}p < 0.01$, $^{***}p < 0.001$.

(C) Schematic of the left and right PLM (presynaptic, magenta) and AVA (postsynaptic, green) neurons. Indicated are the three types of synapses (PLM, Neighbor, and Distal) analyzed in the synaptic plasticity experiments.

(D and G) Confocal images of either SEP::GLR-1 (D) or GLR-1::GFP (G) in the distal processes of the AVA neurons and VAMP::mCherry in presynaptic PLM neurons in transgenic worms that also expressed ChIEF. The distal processes were imaged, as this is the location of synaptic contacts between PLM and AVA. Shown are images from worms either with or without 1 hr optogenetic training (see Experimental Procedures). Both VAMP::mCherry and ChIEF were expressed presynaptically in mechanosensory neurons, including PLM, using the *mec-3* promoter. Red arrowheads (PLM) indicate PLM synapses that expressed either SEP::GLR-1 or GLR-1::GFP postsynaptically, yellow arrowheads (Neighbor) indicate SEP::GLR-1 or GLR-1::GFP puncta in close proximity to PLM puncta, and light blue arrowheads (Distal) indicate SEP::GLR-1 or GLR-1::GFP puncta located distal to PLM puncta. White dashed boxes indicate the SEP puncta shown in (F) or the GFP puncta shown in (I). Scale bar indicates 5 μm.

(E and H) Quantification of SEP::GLR-1 (E) and GLR-1::GFP (H) fluorescence of single puncta at PLM (red arrowheads), neighboring (yellow arrowheads), and distal (light blue arrowheads) synapses. n > 10 (E); n > 15 (H). $^{*}p < 0.05$ and $^{***}p < 0.001$.

(F) Higher magnification of individual SEP::GLR-1 puncta shown in (D).

(I) Higher magnification of individual GLR-1::GFP puncta shown in (G).

EXPERIMENTAL PROCEDURES

Strains and Genetics

All *C. elegans* strains were raised under standard conditions on the *E. coli* strain OP50 at 20°C unless otherwise noted. Wild-type worms were the Bristol N2 strain. Mutant alleles used were *glr-1(ky176)* (Maricq et al., 1995), *glr-2(ak10)* (Mellem et al., 2002), *unc-116(wy270)* (loss-of-function allele) (Yan et al., 2013), *unc-116(rh24)* (Byrd et al., 2001), *klc-2(km11)* (Byrd et al., 2001), *unc-43(n498n1186)* (loss-of-function allele), *unc-43(n498sd)* (gain-of-function allele) (Park and Horvitz, 1986), *eat-4(ky5)* (Lee et al., 1999), *unc-2(ox2)* (Schafer and Kenyon, 1995), *egl-19(n582)* (Lee et al., 1997), and *unc-36(e251)* (Schafer et al., 1996). Plasmids, transgenic arrays, and strains are described in the Supplemental Experimental Procedures. All fluorescently labeled proteins were found to be functional in transgenic rescue experiments of the mutant phenotype.

Confocal Microscopy

Worms were mounted on 10% agarose pads with 1 μl of 30 mM muscimol unless otherwise indicated. Streaming imaging and analysis were performed as previously described (Hoerndli et al., 2013). All confocal images were acquired using a Nikon Eclipse Ti microscope WaveFX-X1 spinning-disc confocal system (Quorum Technologies) with 491 and 561 excitation lasers (Coherent). Images were captured using two matched Cascade II 1024 EMCCD cameras (Photometrics) with 300 ms exposure times on a Nikon Eclipse Ti with a Nikon 100× 1.49 NA TIRF objective. Image acquisition and device control were enabled by Metamorph 7.7.7 (Molecular Devices).

$HisCl_2$ Treatment and Imaging

Before imaging, worms were transferred to agar plates with food (*E. coli* OP50) that also contained 10 mM $HisCl_2$ for 1 hr. For imaging GLR-1 transport, worms were mounted on microscope slides using muscimol to immobilize the worms as previously described (Hoerndli et al., 2013).

CALI, FRAP, and Photoconversion

CALI inactivation was achieved by exposure to 5–12 mW/mm^2 of 488 nm light from a mixed Argon gas laser for 2–5 min. Light exposure was limited to specific regions (cell body or neural processes) using a Mosaic II digital mirror device (Andor) controlled through MetaMorph. To illuminate the whole field of view, we focused an LED light source (5 mW/mm^2, 457 nm) through the upper condenser lens. For cell body CALI, four 1 min pulses of 488 nm light were delivered at four different focal planes to illuminate the entire volume of the cell body, including parts of the process that entered the nerve ring.

Photobleaching (FRAP) experiments were performed as previously described (Hoerndli et al., 2013). For studies of SEP::mCherry::GLR-1, we photobleached the region of interest (ROI) as well as two fields of view (~120 μm) on either side of the ROI to limit contributions to FRAP from possible diffusion of receptors.

For photoconversion, two to three synaptic puncta (GLR-1::Dendra2) were converted sequentially using a 750 ms pulse of 35 mW/mm^2 from a 405 nm laser. For CALI following photoconversion, the whole field of view was illuminated. Worms were then taken off the microscope slide and allowed to feed for 4 hr at room temperature (protected from light exposure) before imaging.

All image analysis was done in Metamorph or ImageJ. A detailed description can be found in Supplemental Experimental Procedures.

Synaptic Plasticity Experiments

L4 transgenic worms were transferred to standard agar plates with food and 450 μM all-*trans*-Retinal overnight (Liewald et al., 2008). A custom array of 457 nm blue LEDs controlled by a Tektronix AFG 3022B pattern generator, delivered 10 ms light pulses at 20 Hz for 30 s every minute with an intensity of 3 mW/mm^2. For image analysis, postsynaptic AMPARs in AVA (marked by SEP or GFP) showing clear overlap with VAMP::mCherry in PLM were identified as PLM synapses (Figures 9C, 9D, and 9G, red arrowheads). We typically identified two synapses in the region with VAMP::mCherry fluorescence that met this criterion, which is consistent with the number of synaptic inputs from PLM to AVA predicted by electron microscopic reconstruction of the *C. elegans* nervous system. PLM also provides synaptic inputs to other neurons in the ventral cord, consistent with the large region of VAMP::mcherry fluorescence (http://wormweb.org/neuralnet#c=PLM&m=1). SEP or GFP puncta underlying VAMP::mCherry, but without overlap, were termed neighboring synapses (Figures 9D and 9G, yellow arrowheads), and SEP or GFP puncta outside of the VAMP::mCherry regions were termed distal synapses (Figures 9D and 9G, light blue arrowheads). Signals were corrected for fluorescence background and quantified in ImageJ.

Antibody Staining

For CypHer experiments, polyclonal anti-HA-CypHer antibodies (Cat. No. 245003Cph from Synaptic Systems) were diluted 1/200 in M9 buffer and injected into the pseudocoelomic space in transgenic *glr-1(ky176)* or *glr-1(ky176); unc-43(lf)* mutants that expressed *Prig-3::HA::glr-1::gfp*. After injection, worms were left to recover on food plates for 1 hr before imaging.

Electrophysiology

Electrophysiological recordings were performed blind to genotype and training condition, using previously described voltage-clamp techniques (Mellem et al., 2002). Currents were evoked by pressure application of 3 mM glutamate, 1 mM NMDA or 200 μM ACh via a Picospritzer II (General Valve) onto the nerve ring as shown (Figure S1A). Cells were held at –60 mV unless otherwise stated. Data were acquired using a HEKA EPC9 amplifier and analyzed using IGOR Pro. All worms expressed GLR-1::GFP in AVA. For CALI experiments, once optimal pipette position was established, the agonist was applied for 500 ms every 60 s. Light from an X-Cite 120 (Exelitas) or through a 100 mW, 457 nm laser (Opto Engine) was continuously delivered at the indicated time points through the objective to the sample at 7–20 mW/mm^2. For analysis of mEPSCs, cells were voltage clamped at –60 mV. Data were sampled at 10 kHz, filtered at 3.3 kHz, and analyzed using IGOR Pro (Wavemetrics) and a suite of custom macros for IGOR written by Dr. Taro Ishikawa (Tarotools, https://sites.google.com/site/tarotoolsregister/contact-me).

Statistical Analysis

The results were analyzed using a Student's t test unless otherwise stated in the figure legends. ANCOVA and linear regression analysis were used to determine statistical differences in SEP and mCherry FRAP, and peak currents after CALI of miniSOG::UNC-43. ANOVA, linear regression, and ANCOVA analyses were performed using Prism 6.0.

SUPPLEMENTAL INFORMATION

Supplemental Information includes Supplemental Experimental Procedures and nine figures and can be found with this article online at http://dx.doi.org/10.1016/j.neuron.2015.03.011.

ACKNOWLEDGMENTS

We thank members of the A.V.M. laboratory for comments on the manuscript, Dane Maxfield and Aleksander Maricq for help with MATLAB analysis, Linda Hauth for generating transgenic strains, Mark Hauth for technical assistance and the *Caenorhabditis* Genetics Center, which is funded by NIH Office of Research Infrastructure Programs (P40 OD010440), and Kang Shen for providing worm strains. This research was made possible by support from NIH Grants NS35812 and DA035080 (A.V.M.) and by postdoctoral fellowships from the Swiss National Science Foundation (F.J.H.).

Received: June 21, 2014
Revised: January 20, 2015
Accepted: February 25, 2015
Published: April 2, 2015

REFERENCES

Anggono, V., and Huganir, R.L. (2012). Regulation of AMPA receptor trafficking and synaptic plasticity. Curr. Opin. Neurobiol. *22*, 461–469.

Bingol, B., Wang, C.F., Arnott, D., Cheng, D., Peng, J., and Sheng, M. (2010). Autophosphorylated CaMKIIalpha acts as a scaffold to recruit proteasomes to dendritic spines. Cell *140*, 567–578.

Brockie, P.J., Mellem, J.E., Hills, T., Madsen, D.M., and Maricq, A.V. (2001). The C. elegans glutamate receptor subunit NMR-1 is required for slow NMDA-activated currents that regulate reversal frequency during locomotion. Neuron *31*, 617–630.

Brockie, P.J., Jensen, M., Mellem, J.E., Jensen, E., Yamasaki, T., Wang, R., Maxfield, D., Thacker, C., Hoerndli, F., Dunn, P.J., et al. (2013). Cornichons control ER export of AMPA receptors to regulate synaptic excitability. Neuron *80*, 129–142.

Byrd, D.T., Kawasaki, M., Walcoff, M., Hisamoto, N., Matsumoto, K., and Jin, Y. (2001). UNC-16, a JNK-signaling scaffold protein, regulates vesicle transport in C. elegans. Neuron *32*, 787–800.

Davis, G.W. (2006). Homeostatic control of neural activity: from phenomenology to molecular design. Annu. Rev. Neurosci. *29*, 307–323.

Davis, G.W. (2013). Homeostatic signaling and the stabilization of neural function. Neuron *80*, 718–728.

de Bono, M., and Maricq, A.V. (2005). Neuronal substrates of complex behaviors in C. elegans. Annu. Rev. Neurosci. *28*, 451–501.

Dolphin, A.C. (2013). The $\alpha 2\delta$ subunits of voltage-gated calcium channels. Biochim. Biophys. Acta *1828*, 1541–1549.

Feinberg, E.H., Vanhoven, M.K., Bendesky, A., Wang, G., Fetter, R.D., Shen, K., and Bargmann, C.I. (2008). GFP Reconstitution Across Synaptic Partners (GRASP) defines cell contacts and synapses in living nervous systems. Neuron *57*, 353–363.

Goold, C.P., and Nicoll, R.A. (2010). Single-cell optogenetic excitation drives homeostatic synaptic depression. Neuron *68*, 512–528.

Granger, A.J., Shi, Y., Lu, W., Cerpas, M., and Nicoll, R.A. (2013). LTP requires a reserve pool of glutamate receptors independent of subunit type. Nature *493*, 495–500.

Gurskaya, N.G., Verkhusha, V.V., Shcheglov, A.S., Staroverov, D.B., Chepurnykh, T.V., Fradkov, A.F., Lukyanov, S., and Lukyanov, K.A. (2006). Engineering of a monomeric green-to-red photoactivatable fluorescent protein induced by blue light. Nat. Biotechnol. *24*, 461–465.

Hart, A.C., Sims, S., and Kaplan, J.M. (1995). Synaptic code for sensory modalities revealed by C. elegans GLR-1 glutamate receptor. Nature *378*, 82–85.

Hell, J.W. (2014). CaMKII: claiming center stage in postsynaptic function and organization. Neuron *81*, 249–265.

Hoerndli, F.J., Maxfield, D.A., Brockie, P.J., Mellem, J.E., Jensen, E., Wang, R., Madsen, D.M., and Maricq, A.V. (2013). Kinesin-1 regulates synaptic strength by mediating the delivery, removal, and redistribution of AMPA receptors. Neuron *80*, 1421–1437.

Hosokawa, T., Mitsushima, D., Kaneko, R., and Hayashi, Y. (2015). Stoichiometry and phosphoisotypes of hippocampal AMPA-type glutamate receptor phosphorylation. Neuron *85*, 60–67.

Huang, Y., and Mucke, L. (2012). Alzheimer mechanisms and therapeutic strategies. Cell *148*, 1204–1222.

Ibata, K., Sun, Q., and Turrigiano, G.G. (2008). Rapid synaptic scaling induced by changes in postsynaptic firing. Neuron *57*, 819–826.

Jeziorski, M.C., Greenberg, R.M., and Anderson, P.A. (2000). The molecular biology of invertebrate voltage-gated Ca(2+) channels. J. Exp. Biol. *203*, 841–856.

Kennedy, M.J., and Ehlers, M.D. (2011). Mechanisms and function of dendritic exocytosis. Neuron *69*, 856–875.

Kerchner, G.A., and Nicoll, R.A. (2008). Silent synapses and the emergence of a postsynaptic mechanism for LTP. Nat. Rev. Neurosci. *9*, 813–825.

Kessels, H.W., and Malinow, R. (2009). Synaptic AMPA receptor plasticity and behavior. Neuron *61*, 340–350.

Lee, R.Y., Lobel, L., Hengartner, M., Horvitz, H.R., and Avery, L. (1997). Mutations in the alpha1 subunit of an L-type voltage-activated Ca2+ channel cause myotonia in Caenorhabditis elegans. EMBO J. *16*, 6066–6076.

Lee, R.Y., Sawin, E.R., Chalfie, M., Horvitz, H.R., and Avery, L. (1999). EAT-4, a homolog of a mammalian sodium-dependent inorganic phosphate cotransporter, is necessary for glutamatergic neurotransmission in caenorhabditis elegans. J. Neurosci. *19*, 159–167.

Liewald, J.F., Brauner, M., Stephens, G.J., Bouhours, M., Schultheis, C., Zhen, M., and Gottschalk, A. (2008). Optogenetic analysis of synaptic function. Nat. Methods *5*, 895–902.

Lin, J.Y., Lin, M.Z., Steinbach, P., and Tsien, R.Y. (2009). Characterization of engineered channelrhodopsin variants with improved properties and kinetics. Biophys. J. *96*, 1803–1814.

Lin, J.Y., Sann, S.B., Zhou, K., Nabavi, S., Proulx, C.D., Malinow, R., Jin, Y., and Tsien, R.Y. (2013). Optogenetic inhibition of synaptic release with chromophore-assisted light inactivation (CALI). Neuron *79*, 241–253.

Malenka, R.C., and Bear, M.F. (2004). LTP and LTD: an embarrassment of riches. Neuron *44*, 5–21.

Mao, L., Takamiya, K., Thomas, G., Lin, D.T., and Huganir, R.L. (2010). GRIP1 and 2 regulate activity-dependent AMPA receptor recycling via exocyst complex interactions. Proc. Natl. Acad. Sci. USA *107*, 19038–19043.

Maricq, A.V., Peckol, E., Driscoll, M., and Bargmann, C.I. (1995). Mechanosensory signalling in C. elegans mediated by the GLR-1 glutamate receptor. Nature *378*, 78–81.

Mellem, J.E., Brockie, P.J., Zheng, Y., Madsen, D.M., and Maricq, A.V. (2002). Decoding of polymodal sensory stimuli by postsynaptic glutamate receptors in C. elegans. Neuron *36*, 933–944.

Nicoll, R.A., and Roche, K.W. (2013). Long-term potentiation: peeling the onion. Neuropharmacology *74*, 18–22.

Park, E.C., and Horvitz, H.R. (1986). Mutations with dominant effects on the behavior and morphology of the nematode Caenorhabditis elegans. Genetics *113*, 821–852.

Pokala, N., Liu, Q., Gordus, A., and Bargmann, C.I. (2014). Inducible and titratable silencing of Caenorhabditis elegans neurons in vivo with histamine-gated chloride channels. Proc. Natl. Acad. Sci. USA *111*, 2770–2775.

Reiner, D.J., Newton, E.M., Tian, H., and Thomas, J.H. (1999). Diverse behavioural defects caused by mutations in Caenorhabditis elegans unc-43 CaM kinase II. Nature *402*, 199–203.

Rongo, C., and Kaplan, J.M. (1999). CaMKII regulates the density of central glutamatergic synapses in vivo. Nature *402*, 195–199.

Sankaranarayanan, S., De Angelis, D., Rothman, J.E., and Ryan, T.A. (2000). The use of pHluorins for optical measurements of presynaptic activity. Biophys. J. *79*, 2199–2208.

Schafer, W.R., and Kenyon, C.J. (1995). A calcium-channel homologue required for adaptation to dopamine and serotonin in Caenorhabditis elegans. Nature *375*, 73–78.

Schafer, W.R., Sanchez, B.M., and Kenyon, C.J. (1996). Genes affecting sensitivity to serotonin in Caenorhabditis elegans. Genetics *143*, 1219–1230.

Setou, M., Seog, D.H., Tanaka, Y., Kanai, Y., Takei, Y., Kawagishi, M., and Hirokawa, N. (2002). Glutamate-receptor-interacting protein GRIP1 directly steers kinesin to dendrites. Nature *417*, 83–87.

Shonesy, B.C., Jalan-Sakrikar, N., Cavener, V.S., and Colbran, R.J. (2014). CaMKII: a molecular substrate for synaptic plasticity and memory. Prog. Mol. Biol. Transl. Sci. *122*, 61–87.

Shu, X., Lev-Ram, V., Deerinck, T.J., Qi, Y., Ramko, E.B., Davidson, M.W., Jin, Y., Ellisman, M.H., and Tsien, R.Y. (2011). A genetically encoded tag for correlated light and electron microscopy of intact cells, tissues, and organisms. PLoS Biol. *9*, e1001041.

Südhof, T.C. (2013). Neurotransmitter release: the last millisecond in the life of a synaptic vesicle. Neuron *80*, 675–690.

Tatavarty, V., Sun, Q., and Turrigiano, G.G. (2013). How to scale down postsynaptic strength. J. Neurosci. *33*, 13179–13189.

Turrigiano, G.G. (2008). The self-tuning neuron: synaptic scaling of excitatory synapses. Cell *135*, 422–435.

Walker, C.S., Brockie, P.J., Madsen, D.M., Francis, M.M., Zheng, Y., Koduri, S., Mellem, J.E., Strutz-Seebohm, N., and Maricq, A.V. (2006a). Reconstitution of invertebrate glutamate receptor function depends on stargazin-like proteins. Proc. Natl. Acad. Sci. USA *103*, 10781–10786.

Walker, C.S., Francis, M.M., Brockie, P.J., Madsen, D.M., Zheng, Y., and Maricq, A.V. (2006b). Conserved SOL-1 proteins regulate ionotropic glutamate receptor desensitization. Proc. Natl. Acad. Sci. USA *103*, 10787–10792.

Wang, R., Walker, C.S., Brockie, P.J., Francis, M.M., Mellem, J.E., Madsen, D.M., and Maricq, A.V. (2008). Evolutionary conserved role for TARPs in the gating of glutamate receptors and tuning of synaptic function. Neuron *59*, 997–1008.

Wang, R., Mellem, J.E., Jensen, M., Brockie, P.J., Walker, C.S., Hoerndli, F.J., Hauth, L., Madsen, D.M., and Maricq, A.V. (2012). The SOL-2/Neto auxiliary protein modulates the function of AMPA-subtype ionotropic glutamate receptors. Neuron *75*, 838–850.

Way, J.C., and Chalfie, M. (1989). The mec-3 gene of Caenorhabditis elegans requires its own product for maintained expression and is expressed in three neuronal cell types. Genes Dev. *3* (12A), 1823–1833.

Yan, J., Chao, D.L., Toba, S., Koyasako, K., Yasunaga, T., Hirotsune, S., and Shen, K. (2013). Kinesin-1 regulates dendrite microtubule polarity in Caenorhabditis elegans. eLife *2*, e00133.

Zheng, Y., Brockie, P.J., Mellem, J.E., Madsen, D.M., and Maricq, A.V. (1999). Neuronal control of locomotion in *C. elegans* is modified by a dominant mutation in the GLR-1 ionotropic glutamate receptor. Neuron *24*, 347–361.

Zheng, Y., Mellem, J.E., Brockie, P.J., Madsen, D.M., and Maricq, A.V. (2004). SOL-1 is a CUB-domain protein required for GLR-1 glutamate receptor function in C. elegans. Nature *427*, 451–457.

Zheng, Y., Brockie, P.J., Mellem, J.E., Madsen, D.M., Walker, C.S., Francis, M.M., and Maricq, A.V. (2006). SOL-1 is an auxiliary subunit that modulates the gating of GLR-1 glutamate receptors in Caenorhabditis elegans. Proc. Natl. Acad. Sci. USA *103*, 1100–1105.